GEUS Bulletin

RESEARCH ARTICLE

Piggyback imbrications, duplex stacking and sequential superimposed deformation in the Fanø Bugt Glaciotectonic Complex, Danish North Sea

Lærke Therese Andersen[1,2]*, Stig A. Schack Pedersen[2]

[1]Department of Geoscience, Aarhus University, Aarhus, Denmark; [2]Near Surface Land and Marine Geology, Geological Survey of Denmark and Greenland, Aarhus, Denmark

Abstract

This study provides a detailed structural analysis of a selected part of the Fanø Bugt Glaciotectonic Complex in the south-eastern part of the Danish North Sea. The 200 km^2 study area was mapped in 3D using high-resolution, 2D multichannel seismic data. The interpretation of seismic profiles demonstrates an architecture markedly separated into a lower and an upper thrust fault level, separated by the upper décollement surface. The lower level is characterised by >15 thrust sheets, with crests that form subsurface ridges with reliefs up to 150 m, scattered over *c.* 15 km. The upper level is characterised by thrust sheets grouped in imbricate complexes with thrust faults connecting to the upper décollement. The structural style changes in the direction of transport, possibly related to the position of the ice-sheet margin responsible for the thrusting and changes in the properties of the basal décollement. The structural style is generally large-scale thrusting and folding, suggesting proglacial deformation. However, the hinterland of the upper thrust fault level displays heavily folded layers or a chaotic reflection pattern associated with subglacial deformation. Special attention is drawn to two exceptional structural frameworks containing a hidden hill-hole pair: SF1, an imbricate thrust fault fan in a 5 km long and 2.5 km wide basin, developed above an extensional normal fault imbricate, and SF2, a frontal ramp uplifting an imbricated fan *c.* 90 m above the average level of thrusting. Restored cross-sections demonstrate a shortening of the lower thrust fault level between 9–43% and 44–49% of the upper level across SF1 and SF2, respectively. We suggest that the glaciotectonic complex was formed proglacially due to gravity spreading in front of an ice margin. Gravity gliding due to an inclined décollement surface of 0.5° and elevated porewater pressure at the décollement might also have facilitated the deformation.

***Correspondence:** *laerketherese@gmail.com*
Received: 01 Dec 2024
Revised: 04 May 2025
Accepted: 11 Jun 2025
Published: 06 Nov 2025

Keywords: seismic interpretation, multiple detachment levels, hill-hole pair, gravity spreading, gravity gliding, thin-skinned thrust-faulting

Abbreviations:
DWTFB: deepwater thrust fault belts
ITFL: intermediate trust fault level
LTFL: lower thrust fault level
UTFL: upper thrust fault level
SF1: structural framework 1
SF2: structural framework 2
S.P.: shot point
TWT: two-way traveltime

Edited by: Kristian Svennevig (GEUS, Denmark)

Reviewed by: David Colin Tanner (LIAG Institute for Applied Geophysics, Germany) and one anonymous reviewer

Funding: See page 18

Competing interests: See page 18

Additional files: None provided

1. Introduction

Glaciotectonic structures are, together with erosional and depositional features, the primary evidence of former glaciation (Aber & Ber 2007). Glaciotectonic complexes provide a record of the nature of the deformation made by various ice advances that formed the surface morphology.

In a glacial setting, gravity-spreading caused by the load of the ice sheet and frictional drag caused by the motion of the ice sheet are the driving mechanisms for the deformation of the substratum (Pedersen 1987, 1996, 2000; Aber *et al*. 1989; Hart 1994; Boulton & Caban 1995; Klint & Pedersen 1995). The resulting deformation creates various structural styles in relation to the position of the ice-sheet margin. Structural styles that appear in the proglacial zone differ from those formed by shearing at the sole in the subglacial zone (e.g. Hart & Boulton 1991; Kupetz 2001; Andersen *et al*. 2005; Pedersen 2014).

In the proglacial zone, deformation is the result of longitudinal compressive stress in front of an ice sheet (e.g. Aber *et al*. 1989; Boulton & Caban 1995; Andersen *et al*. 2005). The structural styles of this zone are associated

with both ductile deformation (i.e. folding) and brittle deformation (i.e. thrusting), depending upon the rheology and competence of the sediments and the behaviour of the ice sheet (Hart & Boulton 1991; van der Wateren 1995). Considering the development of fold and thrust structures in glaciotectonics, it is at present regarded as being the result of fault-propagation folding (Brandes & Le Heron 2010).

In the subglacial zone, deformation is the result of frictional drag beneath the ice sheet due to the ice-sheet movement and extension caused by its load (Moran 1971; Hart & Boulton 1991; Boulton & Caban 1995; van der Wateren 1995; Pedersen 1996, 2000; Andersen *et al*. 2005). The resulting structural styles include folded, often refolded, pervasively sheared or chaotically mixed sediments (Aber 1985), boudinage structures (Berthelsen 1979) and listric normal fault imbricates (Croot 1987). High porewater pressure below the snout of the ice sheet may reduce the effective load of the ice sheet to zero. This will force the proglacial compressional zone to move up-glacier to the point where the load of the ice sheet is being exerted on the subsurface again. Hence, compression can occur below the ice-sheet margin (Boulton & Caban 1995; Andersen *et al*. 2005).

The existence of a décollement horizon at a suitable depth in the subsurface sediments is of great importance for the development of glaciotectonic structures (e.g. van der Wateren 1985; Huuse & Lykke-Andersen 2000a; Andersen *et al*. 2005). The rheology of the décollement surface and circumstances that can alter it, such as permafrost or high porewater pressure, determine the efficiency of the décollement surface (Boulton & Caban 1995; Boulton *et al*. 1999). Porewater flow and the derived elevated groundwater pressure facilitate the formation of décollement surfaces in a glacial setting (Mathews & Macay 1960; Boulton & Caban 1995; Boulton *et al*. 1999).

A dipping décollement surface may induce the mechanism of gravity gliding and contribute to deformation. Structural styles such as a linkage of up-dip extension with down-dip contraction via a detachment zone is usually associated with the mechanism of gravity gliding (Morley *et al*. 2011). According to Hubbert & Rubey (1959), an inclination of 0.5° is enough to facilitate gravity gliding.

Glaciotectonic deformation is like other compressional crustal disturbances, the only significant differences being temporal and spatial scales. In general, the size of the structures and depth of deformation are related to the size of the advancing load and the time interval during which the load was effective in reducing shear strength of the deformed material. Displacement above a décollement with elevated hydrostatic pressure is essential in glaciotectonic deformation as well as in other tectonic settings (Aber & Ber 2007). Hence, the thrust fault architecture of proglacial glaciotectonic structures is analogous to tectonic structures in thin-skinned fold and thrust belts that appear in orogenic foreland basins, at accretionary wedges or in the toes of large deltas and landslides. Consequently, the same structural analysis techniques (Dahlstrom 1969; Hossack 1979; Boyer & Elliott 1982; Butler 1987; De Paor 1988; van der Pluijm & Marshak 2004) can be applied to interpret glaciotectonic structures (e.g. Pedersen 1987, 1996, 2005, 2014; Hart 1990; Klint & Pedersen 1995; van der Wateren 1995; Boulton *et al*. 1999; Phillips *et al*. 2018).

Offshore mapping of the subsurface is often carried out using seismic data. Applying this method to the investigation of glaciotectonic thrust fault complexes has advantages and disadvantages. Often the seismic data can reveal the remains of the entire glaciotectonic complex from base to top. Several profiles across the glaciotectonic complex give a good basis for performing a 3D geometric analysis and describing the internal architecture and structural styles of the thrust structures (e.g. Høyer *et al*. 2013; Pedersen & Boldreel 2017; Vaughan-Hirsch & Phillips 2017; Phillips *et al*. 2018; Winsemann *et al*. 2020; Lohrberg *et al.* 2022). However, the seismic method has its limitations. The horizontal and vertical resolutions of seismic data are primarily controlled by the Fresnel zone and the bandwidth of the seismic source, respectively. Furthermore, steeply dipping layers or faults may not be accurately resolved, as reflections from high-angle features may fall outside the recording aperture (Yilmaz 1987). Hence, features smaller than the seismic resolution, and nearly vertical layers or steeply dipping faults recognised in many of the onshore coastal profiles of glaciotectonic complexes (Rosenkrantz 1944; Steinicke 1972; Pedersen 2000, 2005; Burke *et al*. 2009; Phillips *et al*. 2018; Gehrmann *et al*. 2019) may not be detected or imaged correctly in the seismic profiles.

This study is focused on an area of 200 km^2 of the Fanø Bugt Glaciotectonic Complex in the south-eastern Danish North Sea (Fig. 1). The aim is: (1) to use high-resolution marine multichannel reflection seismic data to map and describe the detailed geometry, architecture and structural styles of the deformation framework present in the investigated area; (2) to conduct a structural analysis on two exceptional structural 'sub-complexes', named the structural framework 1 (SF1), situated in the centre of the area, and the structural framework 2 (SF2), situated at the mid-northern boundary of the investigated area (Fig. 1). From these two 'sub–complexes', the structural analysis is directed towards the development of a kinematic model that supports the structural evolution of the investigated part of the Fanø Bugt Glaciotectonic Complex; (3) to discuss and suggest the possible formation mechanisms related to the mapped architecture and structural styles of the deformations.

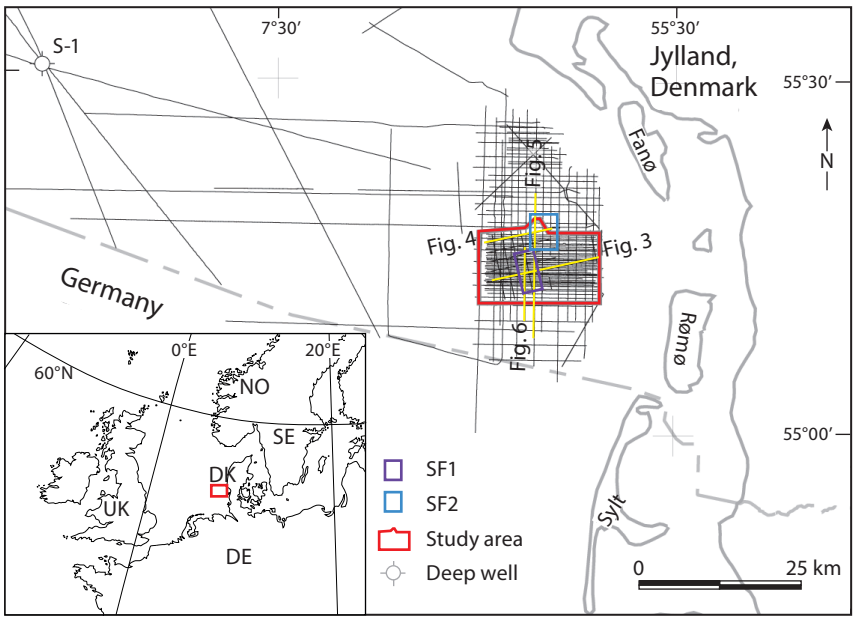

Fig. 1 Location in the south-east Danish North Sea of the Fanø Bugt Glaciotectonic Complex and the seismic lines used for interpretation. The 10 × 20 km² study area is marked with a red rectangle. Locations of the two structural frameworks SF1 and SF2 are marked with purple and blue rectangles, respectively. Locations of seismic lines shown in Figs 3–6 are outlined in yellow.

2. Geological setting

The Fanø Bugt Glaciotectonic Complex is situated in the south-eastern part of the Danish North Sea, 25 km off the west coast of south-west Jylland, Denmark, and covers an area of more than 600 km² (Fig. 1). The western border of the thrust complex can be mapped within the extent of the seismic data, but towards the east, north-east and south-east, the seismic sections reveal that the thrust complex extends farther towards the coast of Jylland (Andersen 2004). This study concerns only a minor part of the Fanø Bugt Glaciotectonic Complex (200 km²), where the seismic lines are spaced close enough to map details of individual structures.

The successions affected by the glaciotectonic deformation consist of Neogene silts and clays of late Burdigalian and younger age (Fig. 2). These sediments were deposited as a progressing accretion sourced from onshore areas of southern Norway and Sweden (Huuse 2002). During the early Miocene, sedimentation in the study area was dominantly shallow marine and terrestrial (Rasmussen 1996, 2004; Rasmussen *et al*. 2010). A regional transgression in the middle Miocene changed the depositional environment to a fully marine shelf environment, which led to the deposition of the fine-grained marine sediments of the Hodde and Gram formations (Friis 1995; Huuse 2002; Rasmussen 2004; Rasmussen *et al*. 2010). The youngest Neogene sediments are shallow marine or brackish-water sediments of late Miocene or early Pliocene age (Berthelsen & Kristoffersen 1974; Fig. 2).

The translated, faulted and folded sediments in the Fanø Bugt Glaciotectonic Complex detach on a *c*. 0.5° westward-inclined basal décollement surface located in the Lower Miocene succession (Andersen 2004). The surface, which in part constitutes the basal décollement surface, displays a regional dip towards the west and south-west of the Cenozoic succession in the eastern Danish North Sea (Huuse *et al*. 2001). The main cause for this is the post-Danian subsidence centred on the Central Graben and late Palaeogene to recent uplift of Fennoscandia (Jordt *et al*. 1995; Japsen 1998; Michelsen *et al*. 1999). Several other thrust complexes in the Eastern North Sea detach in Miocene sediments (Huuse & Lykke-Andersen 2000a; Lohrberg *et al.* 2022). A common feature for several of these complexes – including the Fanø Bugt Glaciotectonic Complex – is that their direction of thrusting is almost parallel to the dip of the décollement surface (Huuse & Lykke-Andersen 2000a).

Mid-latitude ice sheets transgressed parts of the North Sea and melted back several times during the Elsterian and the Saalian glaciations, whereas the Weichselian ice sheets only reached the northern part of the North Sea (Ehlers 1990; Houmark-Nielsen 2011). A succession of tills from the Elsterian and Saalian glaciations and fine-grained interglacial sediments from the Holsteinian and the Eemian succeeded the Neogene deposits (Knudsen & Penny 1987; Sha *et al*. 1991). Quaternary buried valleys cutting both the Neogene and Quaternary successions are recognised in several places in the North Sea (Salomonsen 1995; Huuse & Lykke-Andersen 2000b; Andersen *et al*. 2013; Steward et al. 2013; Prins & Andersen 2019; Lohrberg *et al*. 2020; Ottesen *et al.* 2020; Wenau & Alves 2020) as well as onshore Denmark (Andersen *et al*. 2013; Sandersen & Jørgensen 2017).

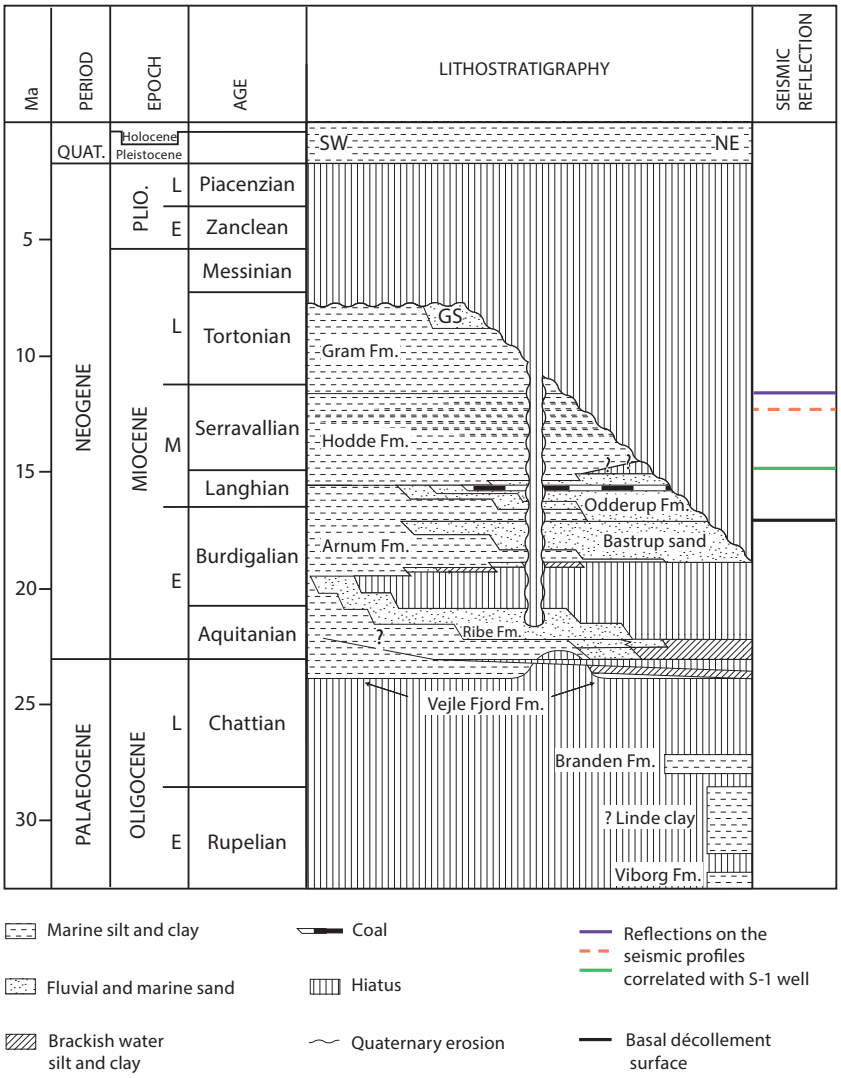

Fig. 2 Stratigraphic diagram (modified from Rasmussen 2004). The succession involved in the thrusting consists of fine-grained sediments (the south-western part of the diagram) of late Burdigalian and younger age. The basal décollement surface (black line) developed in the fine-grained sediments of the Arnum Fm (Early Miocene). The upper décollement surface developed in the fine-grained sediments of the Hodde Fm (Middle Miocene), between the orange and purple reflectors.

The upper boundary of the deformed succession in The Fanø Bugt Glaciotectonic Complex is interpreted to be a Saalian glacial unconformity. This erosional surface forms a hummocky and even hilly landscape with small erosional basins (Larsen & Andersen 2005). The deformation of the glaciotectonic complex is not directly dateable, as no adequate borehole information is available in the Fanø Bugt area. An Elsterian or early Saalian age has been suggested (Huuse & Lykke-Andersen 2000a). Kinetostratigraphic correlation with onshore glaciotectonic deformations of similar size, style and transport direction indicates that the Fanø Bugt Glaciotectonic Complex formed during a stage of westward movement of the Late Saalian (Warthe) ice sheet (Andersen 2004; Houmark-Nielsen 2007; Jørgensen *et al*. 2012). A pre-Elsterian or early Elsterian age of formation has recently been suggested by Winsemann *et al*. (2020), based on a correlation with the glaciotectonic complex at Heligoland in the south-eastern German North Sea.

3. Data and methods

3.1. Seismic data acquisition and parameters

The University of Aarhus and the Geological Survey of Denmark and Greenland (GEUS) acquired the high-resolution marine seismic data on scientific cruises in the North Sea during the years 1999–2001 with the Danish Navy ship, *Flyvefisken*. The seismic data from these surveys, named FL99, FL00 and FL01, were collected to map the area of the Fanø Bugt Glaciotectonic Complex (Andersen 2004). The surveys make up a dense grid of 1065 km long, high-resolution, multichannel-reflection seismic lines, distributed over an area of *c*. 10 × 20 km^2 (Fig. 1). The grid spacing is *c*. 250 m between

approximate dip lines and *c*. 1500 m between approximate strike lines. In addition, a few lines from the surveys DA95 and GR98 (Huuse 2000), which crossed the area, were used, and a few conventional oil-seismic data (RTD–RE94 and NP85N) were used for the correlation of the interpreted horizons to the well S-1 about 70 km west of the study area (Andersen 2004).

The signal bandwidth of the migrated seismic data is 50–180 Hz, and the vertical penetration is 2000 ms two-way traveltime (TWT), corresponding roughly to 2000 m (Clausen & Huuse 1999). The seismic data acquisition was limited towards land by the 10 m water-depth contour, selected as a safety precaution for equipment and ship. The vertical and horizontal resolutions are approximately 5 m and 20 m, respectively. Data quality is generally good; however, interpretation of the top 50–100 ms TWT is often hampered by water-layer multiples. Minor mis-ties between individual surveys and mis-ties due to migration problems in the neighbourhood of steeply dipping faults and associated tilted layers were identified and corrected prior to interpretation. The limited resolution and challenges in imaging steep dips may explain the presence of large areas of chaotic reflection patterns (e.g. Fig. 3, shot point, S.P., 0–730, top half of the profile). It is likely that the structures in this area were either smaller than the seismic resolution (5 m vertical and 20 m horizontal) or that layers or faults were steeply dipping. However, the nature of the deformation can also contribute to obtain a chaotic reflection pattern in areas where structural and sedimentary architecture is particularly complex.

3.2. Interpretation, maps and plots

The seismic data were interpreted digitally using Landmark's Openworks, Seisworks 2D software (2002–2003). Difficulties occurred when interpreting thrust horizons, as the software does not allow multiple TWT values for a single horizon at the same shot point (S.P.). Hence, an advanced interpretation strategy was necessary. As the overlap of a thrust horizon cannot be represented by a single horizon, a new horizon was made where a TWT value occurred at the same S.P. representing the deeper TWT values of overlap between the adjacent thrust sheet. Hence, all the upper TWT values were represented by the same horizon.

Maps of the basal décollement (floor thrust), the upper décollement (roof thrust) and a structural map of an internal reflection in the lower thrust level were drawn using Landmark's Openworks, Z-map+ software. The horizons data were imported from Seisworks and were gridded using the least squares algorithm, with a grid increment on 45 m. Smoothing was performed before contouring with an interval of 10 ms and 20 ms, respectively.

The dip of the basal décollement surface was calculated using a velocity of 1850 m/s and basic trigonometry by the following equation:

$$\tan(A) = a/b \qquad \text{(Eq. 1)}$$

where A = dip angle, b = distance between contours perpendicular to the strike of contours measured on the map. a is defined in Eq. (2) as follows:

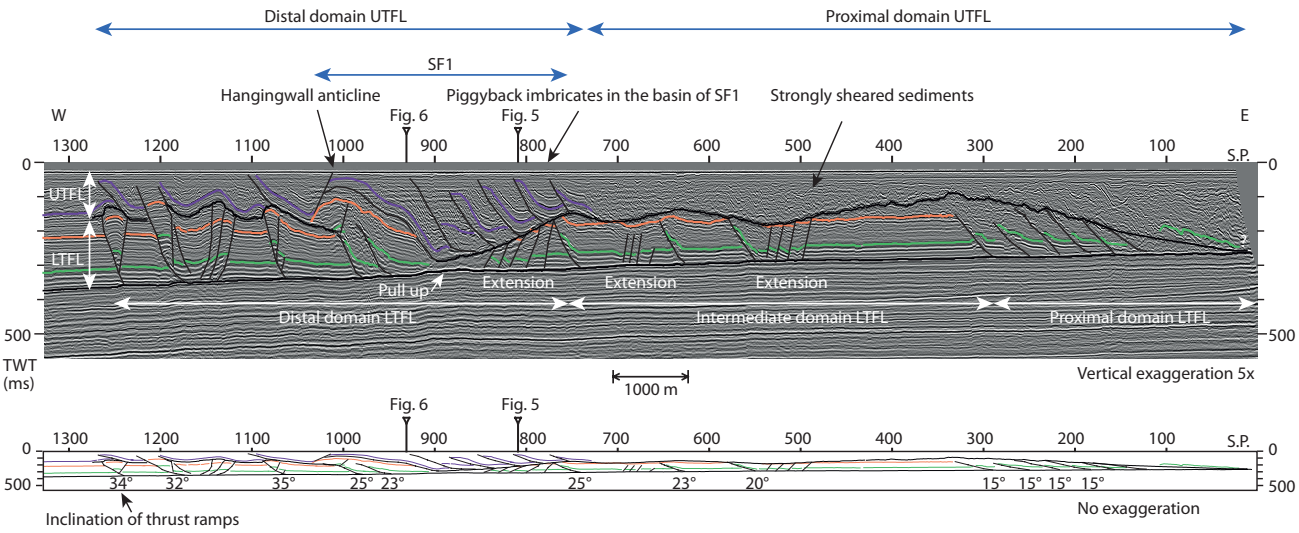

Fig. 3 Seismic section (Fl01–50) showing a duplex with imbricated thrust sheet in two levels. The lower thrust fault level (LTFL) is detaching on the basal décollement surface acting as a floor thrust. The UTFL is detaching on the Upper décollement surface, acting as a roof thrust for the LTFL and a floor thrust for UTFL. LTFL and UTFL can be divided into three and two structural domains, respectively, showing different structural styles (see Section 4.3 and 4.5 and Fig. 8). The seismic section is an approximate dip line to SF1, showing piggyback imbricates in a basin (S.P. 725–900) behind a huge hanging wall anticline (S.P. 900–1050). Seismic section shown with 5x vertical exaggeration. Interpretations shown below the seismic section with no exaggeration. Here, the inclination of the thrust faults ramps is measured. Crossing seismic lines are marked on the seismic section with a figure number, see Figs 1, 7 and 8 for location of this cross-section. **S.P.**: Shot point. **TWT**: Two-way travel time.

$$\alpha = ((\text{ContourTWTmax} - \text{ContourTWTmin})/2) \times \text{velocity} \quad \text{(Eq. 2)}$$

The velocity used here is an average velocity of the Post Chalk Group, based on Nielsen & Japsen (1991). A velocity range of 1700–2000 m/s was considered for uncertainty, resulting in a variation in dip angle of approximately ±0.03°.

Plots of the seismic data and interpretation were produced for illustrations. The vertical scale was calculated using a velocity of 1850 m/s, while the horizontal scale was determined by multiplying the number of traces by the distance between traces. The seismic data plots were produced with a 5x vertical exaggeration. A version without vertical exaggeration, displaying only the interpretation, is presented below the seismic section. This version was created by reducing the vertical scale by a factor of five while preserving the horizontal scale.

3.3. Structural analysis

A structural analysis was conducted based on the mapping and description of horizon topography, thrust fault orientation and geometry of thrust sheets. Restoration of SF1 and SF2 was performed to give a rough estimate of the minimum amount of shortening and to reconstruct the deformational history of SF1 and SF2 in a tentative kinematic model.

The concept for the restoration of the cross-section was based on the method for balanced cross-sections (Dahlstrom 1969; De Paor 1988; Wilkerson & Dicken 2001; van der Pluijm & Marshak 2004). This method assumes constant layer thickness, constant along-strike displacement along faults and plane-strain deformation. We realise that these assumptions cannot all be fulfilled in a glaciotectonic context, and that the limitations of the seismic method have implications for the result.

When performing the structural balancing, it is essential to restore all strains and displacements in the reverse order in which they were applied (Butler 1987). Hence, the restoration was done stepwise, starting with the youngest, westernmost faults in the lower thrust fault level (LTFL) towards the oldest, easternmost faults. The same procedure was performed for the structures in the upper thrust fault level (UTFL), as it was assumed that the UTFL was deformed before the LTFL (see Section 4.6 for more details).

We performed a tentative 2D line-length balancing of the structural interpretation of the two seismic cross-sections, approximate dip lines to SF1 and SF2 (Figs 3 and 4) on the interpreted reflections, the purple reflector in the UTFL and green reflector in LTFL (results in Sections 4.8 and 4.9).

The starting point for the kinematic model was the deformed sections (the interpreted seismic sections) illustrated in the final step of the restoration. From here,

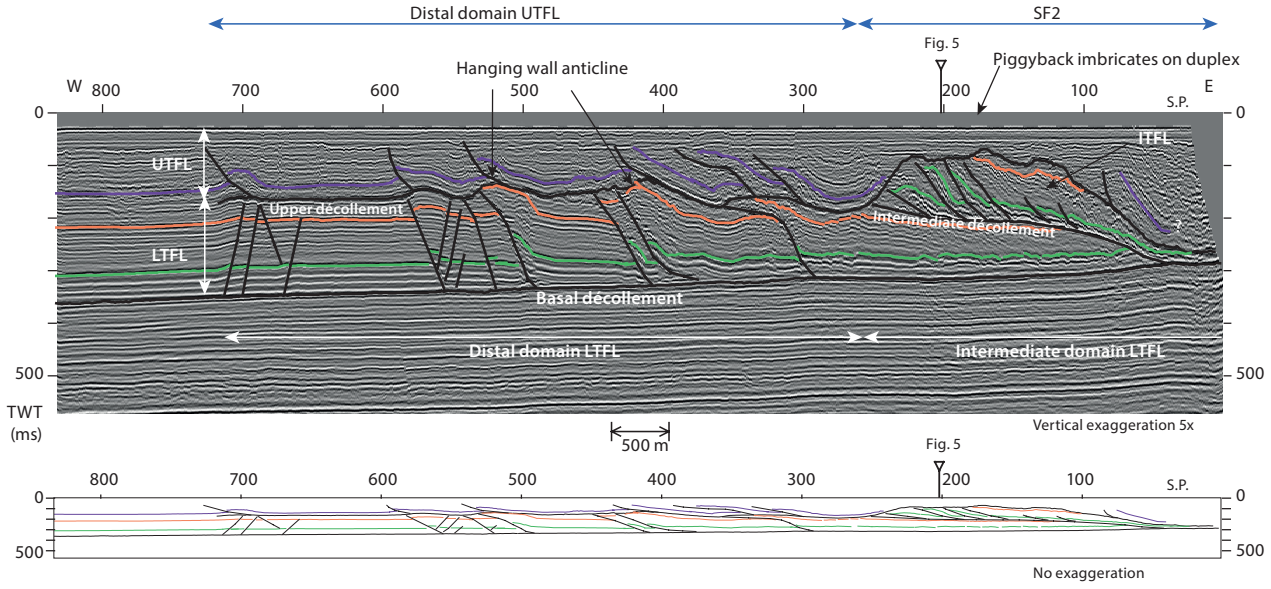

Fig. 4 Seismic section (Fl01–54) showing an approximate dip profile across the structural framework SF2, showing piggyback imbrication of the sedimentary succession of LTFL repeated and uplifted more than 100 ms (*c.* 90 m; see also SF2 in Fig. 8) on a frontal ramp and a flat acting as an intermediate décollement surface for ITFL. West of SF2 is the general duplex of the area with large-scale thrust structures (some more than 1000 m long) in LTFL and UTFL translating across the basal décollement and upper décollement, respectively. Hanging wall anticlines in LTFL is superimposed in the upper décollement as folding of the surface. Small-scale structures can be seen in the hinterland part of the cross-section but cannot be outlined accurately. Seismic section shown with 5x vertical exaggeration. Interpretations shown below the seismic section with no exaggeration. Crossing seismic lines are marked on the seismic section with a figure number. See Figs 1, 7 and 8 for location of this cross-section. **S.P.**: Shot point. **TWT**: Two-way travel time.

the model progresses stepwise up to step 1 – the balanced section.

Folding is generally regarded as fault-related; however, in one place, we tentatively interpret the deformation as ductile attributed to hydrodynamic shear deformation (see section 4.9; Step 3, top of $SF1_3$). A sediment package subject to hydrodynamic shear deformation could potentially spread in multiple directions. Hence, in this case, line balancing is first applied to the tilted normal fault blocks, and the area subjected to hydrodynamic shear deformation is reconstructed to fill in the rest of fault block $SF1_3$.

Since the restoration was performed only on one reflector in each level, the fault dip was preserved as observed in the deformed section throughout the restoration process.

To calculate section shortening, a fixed pin line was placed at the front of each thrust-fault level and a loose pin in the rear. The displacement between the deformed and restored sections provides the average contraction of the upper and lower thrust fault levels, respectively. The calculations were done by measuring the distance between the front (fixed) pin and the rear (loose) pin for each thrust-fault level and for each step, relative to the original length.

Erosion of the top of the sections is not accounted for. Hence, the calculated shortening represents a minimum estimate. An exception is the westernmost fault block of the UTFL in SF1, where an eroded fault block segment is added to maintain the front pin line position, as this fault block is moved eastward during the restoration of the LTFL from step 4 to step 3 (see section 4.9).

4. Results

4.1. The seismic interpretation

The seismic data quality is generally good and provides many excellent images of the glaciotectonic structures in a large part of the study area. The line spacing in the W–E direction is close enough to trace the largest faults from line to line, providing a good opportunity to describe the geometry, the internal architecture and structural styles of this part of the Fanø Bugt Glaciotectonic Complex.

The interpretation is based on the recognition of distinct reflection patterns; equal thickness of undeformed layers across faults was used in areas where the identification of the reflection pattern was difficult. Ramps of thrust faults or normal faults were mapped where an abrupt cut of reflections occurs in the vertical plane. Thrust-fault flats or décollement surfaces were mapped where more or less horizontal discontinuities existed. These boundaries appeared where undeformed sediments were overlain by deformed sediments, or where different structural patterns were recognised across a horizontal or weakly inclined surface.

Five internal reflections, including two décollement surfaces and numerous thrust faults and normal faults, were interpreted. The following description of the interpreted and mapped surfaces and fault is exemplified on four seismic cross-sections: Two approximate dip sections (Figs 3 and 4) and two sections oblique to strike (Figs 5 and 6) cross the centre of SF1 and SF2, respectively (see Fig. 1 for location). The internal architecture

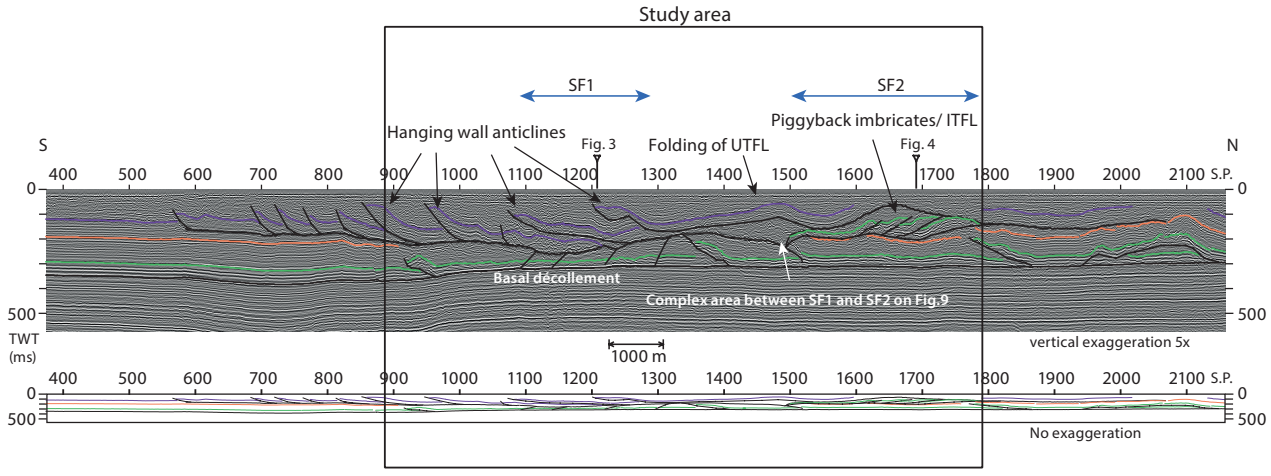

Fig. 5 Seismic section (Fl00–27) is crossing the area oblique to strike of the structural elements and across both SF1 and SF2. The cross-section is showing an apparent 'spreading' of the transport direction of thrust sheets between thrust fault levels. The apparent direction of thrust sheets of UTFL is towards south (S.P. 570–1300). At SF2, the lower succession is repeated in ITFL; here, the apparent thrust direction is towards north (S.P. 1500–1800). The apparent direction of thrusting of LTFL is towards south, ending at S.P. 900. South of the study area, thrusting only appears in the UTFL. Normal faults in the LTFL are seen at SF1 dipping opposite the thrust fault. The UTFL repeats across SF1 (see purple reflector), compare also with dip-section across SF1 (Fig. 3). The true thrust direction can be inferred from Fig. 8. Seismic section shown with x5 vertical exaggeration. Interpretations shown below the seismic section with no exaggeration. Crossing seismic lines are marked on the seismic section with a figure number. See Figs 1, 7 and 8 for location of this cross-section. **S.P.**: Shot point. **TWT**: Two-way travel time.

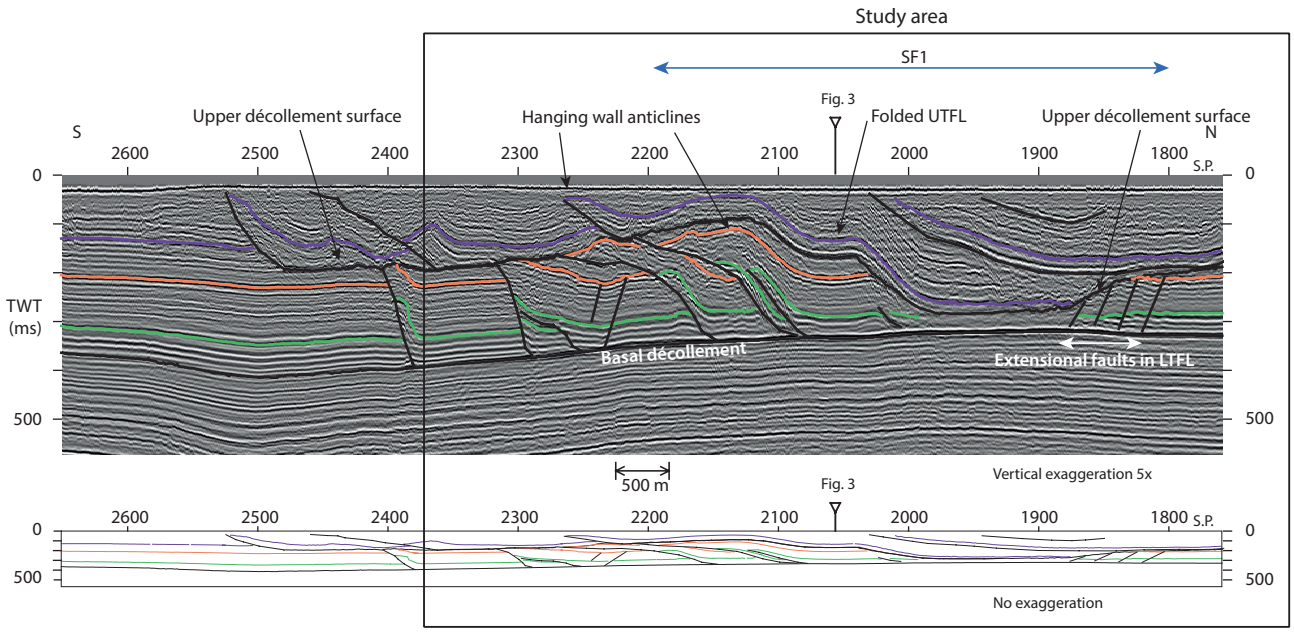

Fig. 6 Seismic section (Fl01–19) is crossing the area oblique to the strike of structural elements and across SF1 at S.P. 1800–2200. LTFL and UTFL show apparent thrusting towards south. Thrusting of UTFL is continuing further towards south (out of the study area) than deformation of LTFL. In the northern part of the profile, extensional faulting is seen in LTFL below the depression of the upper décollement surface. UTFL is repeated in the basin of SF1 (S.P. 1880–2030, see purple reflections). The true thrust direction can be inferred from Fig. 8. Seismic section shown with 5x vertical exaggeration. Interpretations shown below the seismic section with no exaggeration. Crossing seismic lines are marked on the seismic section with a figure number. See Figs 1, 7 and 8 for location of this cross-section. **S.P.**: Shot point. **TWT**: Two-way travel time.

and structural styles seen in these figures are described in the figure caption.

4.2. The mapped surfaces

The lower boundary of the glaciotectonic complex is the basal décollement surface. This surface separates the undeformed layers below from the deformed layers above, see the seismic lines Figs 3–6. The surface that constitutes the basal décollement surface within the study area has been mapped in a larger area, and a TWT map has been generated (Fig. 7). This map is described in Section 4.4.

The layers just above the basal décollement surface have a distinct reflection pattern of several parallel (when not disturbed) very strong reflections. The top reflection of this unit is marked with green in the seismic cross-sections (Figs 3–6). It is possible to follow the green reflector in most of the study area, and a structural TWT map shows the topography of this surface and the thrust fault trends of the LTFL (Fig. 8). A description of this map is given in Section 4.5.

The reflection pattern above the green reflector also consists of parallel reflections, although less intense. The orange reflector marks the top of three (sometimes only two) very strong reflectors in the upper part of the LTFL (Figs 3–6). Because of disturbance due to deformation, it has only been possible to map this surface in parts of the study area, and no resulting topographic map has been generated.

The roof thrust of the LTFL appears above the orange reflector. We refer to it as the upper décollement surface (Figs 3–6). Above this surface, there is the UTFL. The upper décollement surface sometimes displays a very strong reflection, and in other parts, it was mapped where a marked change in structural styles appears above and below the surface. A perspective view of this décollement surface is seen in Fig. 9 and described in Section 4.6.

In the UTFL, only one reflector was outlined, which, in the seismic cross-sections, is displayed in purple (Figs 3–6). This surface is the reflection from a series of parallel-layered beds above the upper décollement surface. These are easily recognised in the undeformed layers west of the thrust front (Figs 3–6). The interpretation of the purple reflector was hampered by multiples and deformation of the layers, making it difficult to recognise in large parts. Hence, no resulting topographic map was generated of this reflector. Above this surface, the reflection pattern is semi-parallel and generally noisy and often distorted by multiples (Figs 3–6).

The westward continuation of the basal décollement surface is stratigraphically located in the Lower Miocene succession (Andersen 2004), and the green, orange and purple reflectors are in the Middle Miocene succession, when correlated with the S-1 well, situated *c.* 70 km NW of the Fanø Bugt Glaciotectonic Complex (Fig. 2). The LTFL is representing the Early/Middle Miocene marine Arnum Formation with possible intercalations of

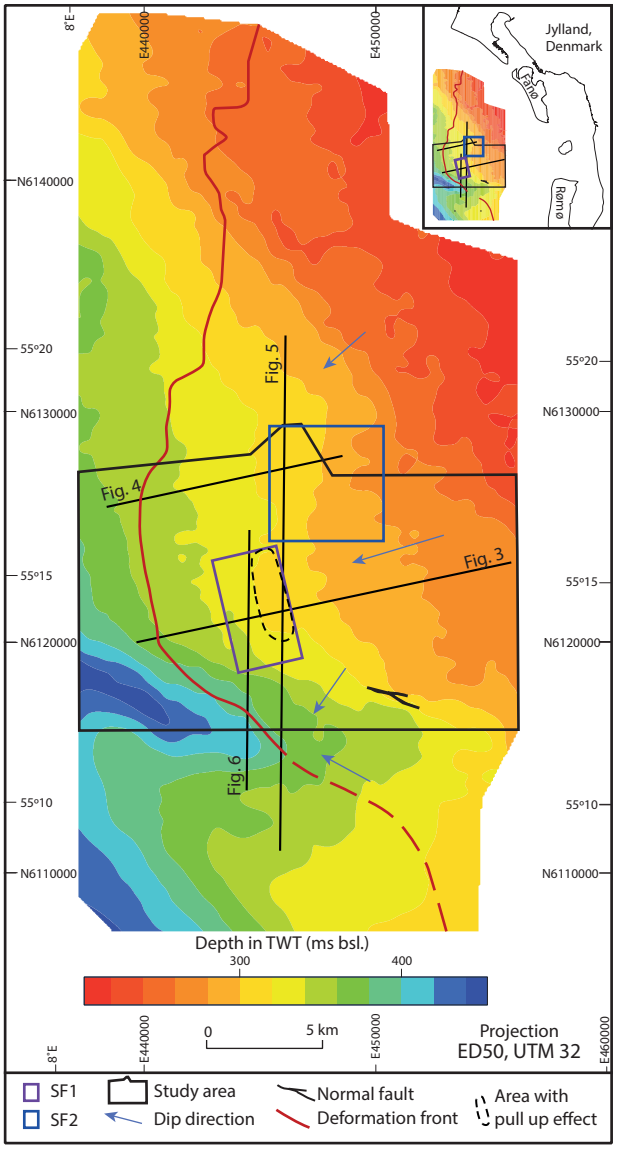

Fig. 7 A two-way time-contour map of the basal décollement surface and its continuation beyond the western limit of LTFL deformation. The deformation front shows that the maximal western extent of the Fanø Bugt Glaciotectonic Complex is situated in the study area. The contour curves of the surface show a marked change in dip and dip direction at the border of the study area (see Section 4.4 for further details). A pull-up of the surface below the basin of SF1 is marked with a black dashed line. Locations of SF1 and SF2 are shown. A small normal fault and a depression of the surface are seen in the southern part of the study area. Seismic sections shown in Figs 3–6 are marked with black lines.

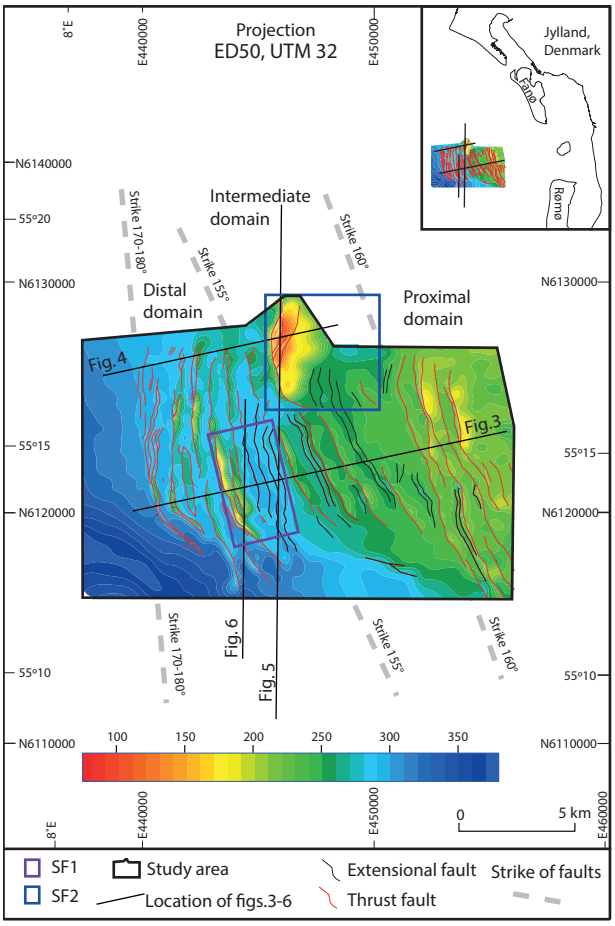

Fig. 8 A structural two-way time (TWT) contour map showing the strike of the main structures at the level of an internal reflection in LTFL and ITFL (green reflector on Figs 3–6). To enhance the overview, the map only shows the larger faults. Thrust faults are marked with red, and normal faults are marked with black lines. The change of strike of faults reveals different structural domains. In the eastern proximal domain, the faults strike 160°, in the intermediate domain, the strike of faults is 155° and in the western distal domain, the strike is 170°–180°. The three structural domains are showing different structural styles (see Section 4.5 and Fig. 3). The trend of the faults is turning in the southern part of the area from west south-west to south-west following the same depression in the surface as is seen in the basal décollement surface (Fig. 7). In the area of SF2, the mapped reflector is elevated c 100 ms (c 90 m) on a huge frontal ramp and flat and display the structural trend of ITFL. The remaining parts of the map show the structural trend of LTFL. The structural trend of ITFL is towards the north-west, hence different to the general structural trend of LTFL, which is towards the west south-west. SF1 displays two huge hanging wall anticlines in front of an extensional basin/depression. The location of SF1 and SF2 is market with rectangles. The seismic sections shown in Figs 3–6 are marked with black lines.

the sandy Bastrup and Odderup Formations, whereas the UTFL constitutes the Middle Miocene, fully marine, clayey Hodde and Gram Formations (Fig. 2). The structural styles of the UTFL are generally more ductile than the deformation in the LTFL, which is interpreted to be due to the different rheology of the sediments.

Thrust-fault trends in the UTFL were mapped from the seismic cross-sections, which provide the transport direction of the thrust sheets (Fig. 10 and Section 4.7). The structures of the UTFL are eroded or truncated at the top by a possible late Saalian unconformity (Larsen & Andersen 2005) or the seafloor (Fig. 3, S.P. 1000–1200).

4.3. Architecture and structural styles

The thrust fault architecture of the study site indicates that the overall geometry is a large-scale duplex with imbricate structures bounded by a floor thrust (the basal décollement) and a roof thrust (the upper décollement).

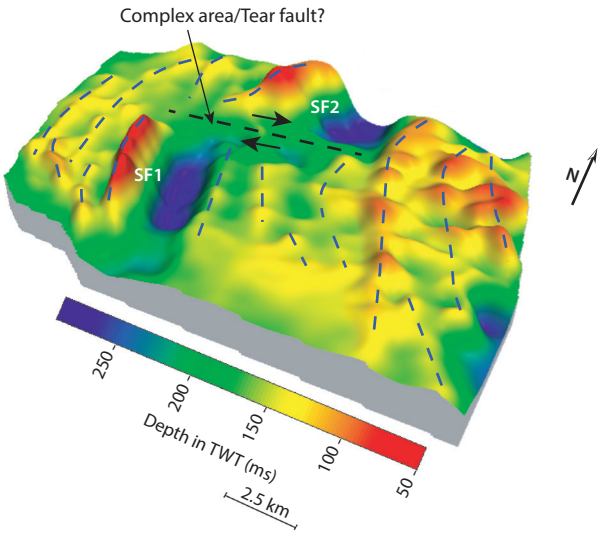

Fig. 9 3D map of the upper décollement surface with a 2.5x exaggeration gives a perspective view of the hilly landscape with ridges above hanging wall anticlines and depressions above extensional faulting in the LTFL. Both SF1 and SF2 comprise hill-hole pairs at this surface level, although the internal structural framework is very different (Figs 3 and 4). SF1 and SF2 are connected by a low-lying area with a complex reflection pattern; hence, the interpretation of this area is uncertain (see Section 4.6). There is a remarkably large coherent ridge just proximal SF1 and SF2.

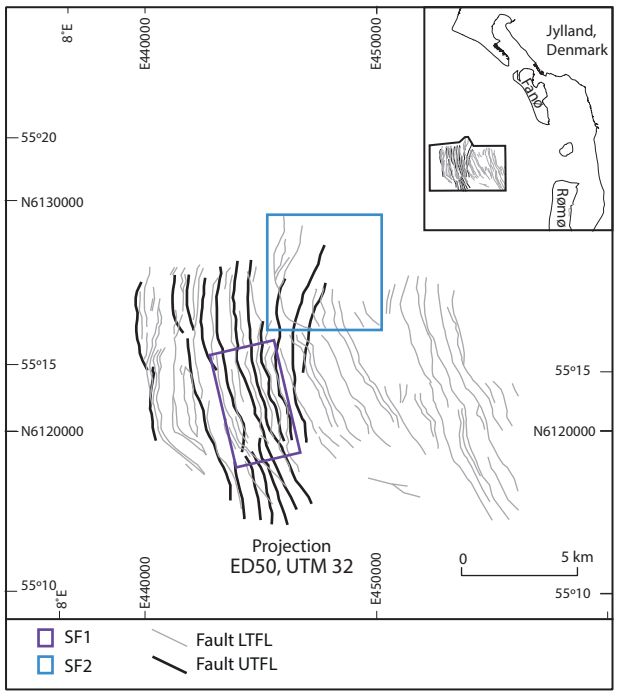

Fig. 10 Map comparing the trends of the faults of the UTFL (black) compared with those of the LTFL (grey), see Section 4.7. The structural trend of the UTFL generally follows that of the LTFL in a smooth manner, for example, across SF2, and the structures of the UTFL connect the two fault directions of LTFL and ITFL in smoothly curving faults. In the south, the bending faults in the LTFL seem to affect the trend of the UTFL much more gently.

The LTFL shows three deformation domains, characterised by different structural styles (Figs 3 and 8) as follows:

1. Small imbricated thrust sheets are seen in the proximal domain to the east (Fig. 3).
2. Larger thrust sheets with tailing tilted normal faults are seen in the intermediate domain (Fig. 3).
3. The distal domain constitutes large thrust sheets with hanging-wall anticlines. Close to the deformation front in the west, back thrusts and pop-up structures dominate the distal domain (Figs 3 and 4).

A more thorough account is presented together with the map of the LTFL (Fig. 8) in Section 4.5.

The succession above the upper décollement surface, the UTFL, displays two different deformation domains: (1) a distal domain with an imbricate system of piggyback thrust structures (Figs 3 and 4); (2) a proximal domain with a diffuse or chaotic reflection pattern (Fig. 3), interpreted to resemble pervasively sheared or chaotically mixed sediments, possibly involving boudinage structures, fluid flow structures and hydrodynamic brecciation.

In the central part of the study area, the structural framework SF1 dominates the seismic images (see dip section in Fig. 3, S.P. 760–1020, sections oblique to strike in Fig. 5, S.P. 1100–1300 and Fig. 6, S.P. 1800–2200), showing a piggyback imbricate fan of the UTFL in a depression 5 km long and 2.5 km wide. Below the piggyback imbricate fan, several partly rotated normal faults are present. In front of the depression, a huge thrust sheet forms a hanging-wall anticline repeating the LTFL in the narrow crest of the anticline (Fig. 3, S.P. 900–1050 and Fig. 6, S.P. 2100–2200).

In the mid-northern part of the study area, another spectacular structural framework is displayed in the seismic sections SF2 (see dip section in Fig. 4, S.P. 0–250 and the section oblique to strike in Fig. 5, S.P. 1500–1800). SF2 consists of a ramp and a flat, along which an imbricate fan of thrust sheets is translated westwards and leaves a tailing depression to the east. The imbricate fan formed by ramp collapse of a thrust segment derived from the LTFL and raised *c*. 90 m above the average level of thrusting in the LTFL. This flat acts as an intermediate décollement surface, and, hence, the imbricated fan represents an intermediate trust fault level (ITFL), situated between an intermediate décollement surface and the upper décollement surface (Fig. 4, S.P. 0–250). The imbricate fan repeats the sedimentary succession of the LTFL in an area of approximately 8.5 km^2, which now comprises a structural high (see SF2 in Fig. 8). The eastern part of SF2 is seen as a depression at the level of the green reflection, which

is partly due to extensional faulting of the LTFL (Fig. 8) and partly caused by the removal of material due to the thrust-sheet translation described earlier (Figs 4 and 8).

4.4. The basal décollement surface

A time-contour map of the basal décollement surface is presented in Fig. 7.

North of the study area and in the north-eastern corner of the study area, the surface dips towards south-west. Inside the study area, the dip is gentler towards west-south-west, changing to south-south-west in the south. South of the study area, the surface dips towards north-west and south-west due to a depression in the surface (Fig. 7).

The strike of the contours changes from *c.* 155° to 160° at the 280 ms TWT curve in the hinterland to *c.* 170° at the 340 ms TWT curve in the foreland. Furthermore, a change in dip angle characterises the transition from the hinterland with low dip (*c.* 0.3°) in the east to a slightly steeper dip towards the foreland (*c.* 0.4°–0.6°). The steepest dip is just east of SF1. In the south-west, the contours change direction again due to a depression of the surface in the south-western corner, and the dip increases to *c.* 1.5° (Fig. 7). This depression and the small normal fault in the southern part of the study area are also seen in the Top Chalk surface (Clausen & Huuse 1999).

The contour curve at 320 ms TWT of the basal décollement surface makes an upward bulge just at the base of SF1, marked with an elongate circle of black dots in Fig. 7. This is presumably a 'pull-up' effect caused by higher seismic velocities in the piggyback-imbricate thrust sheets filling the basin (Fig. 3, S.P. 850-925). In the surrounding area, the décollement surface is relatively smooth, with no obvious indications of a real bulge on the décollement surface. The existence of velocity pull-up is supported by the seismic image in Fig. 3 (see basal décollement, S.P. 850–925).

The deformation front of the LTFL (Fig. 7) marks the transition from the deformed frontal part of the complex to the undeformed foreland towards west. The deformation front reaches its maximal western extent in the study area (Fig. 7). Towards the south-west, the deformations reach their maximum depth and coincide approximately with the 400 ms TWT contour curve of the basal décollement (Fig. 7). This may indicate that *c.* 360 m (*c.* 400 ms TWT) is the maximum deformation depth in the Fanø Bugt Glaciotectonic Complex.

4.5. The structural trend of the lower and intermediate thrust fault levels

A structural two-way time-contour map was generated (Fig. 8) to investigate a distinct internal surface in the lower part of the complex (indicated by the top level of the green reflector in Figs 3–6). The map shows both the topography of the surface and the geometry, dimension and transport direction of the structures of the LTFL translated on the basal décollement surface. Furthermore, Fig. 8 shows the structures of the intermediate thrust fault level (ITFL) translated on the intermediate décollement surface at the location of SF2. Thrust faults and back thrusts are displayed by red lines and normal faults with black lines. For an overview, Fig. 8 shows only 25 of the larger faults out of a total of 35 faults shown for the LTFL in Fig. 3.

The fault trend in the LTFL can be divided into three structural domains based on the change in strike of the fault structures (Fig. 8). On the seismic sections, the change in fault strike correlates with a change in structural styles (see LTFL in Fig. 3).

The three structural domains are as follows:

1. The eastern proximal domain consists of a succession of relatively small imbricated thrust sheets striking 160°, with thrust faults dipping *c.* 15° (Fig. 3, S.P. 125–335).

2. In the intermediate domain, a 2 km wide block of more or less undeformed sediments (Fig. 3, S.P. 335–480) constitutes the eastern part of the domain (Fig. 8). Farther west, a succession of larger thrust sheets with tailing extensional listric normal faults exists. The faults are striking 155° (Fig. 8) and dipping *c.* 20°–25° (Fig. 3, S.P. 480–750). The significant structure SF2 is located in the central northern part of the intermediate domain (Fig. 8). Sections crossing this structure are shown in Fig. 4 (S.P. 0–250) and Fig. 5 (S.P. 1500–1800). A correlation of a hill-hole pair is expressed by the depression east of the 'thrust-fault high' (Fig. 8). At the 'thrust-fault high', the LTFL is repeated directly on top of itself with the UTFL above. Hence, at this place, one could argue that a third ITFL is present, which, however, consists of the same sediment package as the LTFL (see e.g. Fig. 4, SF2). The map (Fig. 8) always expresses the upper position of the mapped green horizon, so, in areas where the horizon repeats itself, it is the ITFL, which is represented in the 'thrust-fault high' (Fig. 8). The structural trend of ITFL in SF2 is towards the north-west, which is notably different to the general structural trend of LTFL, which is towards west and west-south-west (Figs 5 and 8).

3. The western distal domain contains faults with a strike direction of 170°–180° (Fig. 8). The significant SF1 appears in this domain (Fig. 3, S.P. 750–1000). In the frontal part, SF1 comprises a more than 1000 m long thrust sheet (Fig. 3, S.P. 900–1000). The inclination of thrust faults in SF1 is 25–23°, the same as for

the structures in the intermediate domain (Fig. 3, S.P. 950–1000). However, in the map view, the strike of the faults in SF1 is the same as for the distal domain (Fig. 8). In the tailing part of SF1, tilted normal faults created a depression (Fig. 3, S.P. 775–900). A spatial view of this depression can be seen in Figs. 8 and 9. This depression covers an area of *c*. 5 km × 2.5 km, where it is most pronounced.

In the distal domain west of SF1, the structural style comprises relatively large thrust sheets with pop-up structures in the frontal part, dipping *c*. 25°–35° (Fig. 3, S.P. 950–1270). These structures delineate the western boarder of the thrust complex (Fig. 8). Small thrusts or reverse faults, with fault planes dipping towards the west, express the thrust front towards the north-western corner of the study area (Fig. 4, S.P. 700). These structures could have started as nucleation points of conjugate contractional faults (Andersen *et al*. 2005), which developed into pop-up structures and fore-thrust/back-thrust pairs during the progressive compressional deformation.

4.6. The upper décollement surface

The upper décollement surface is interpreted to be a decoupling unconformity separating UTFL from LTFL (see Figs 3–6) in most of the study area. A perspective view of the upper décollement surface (Fig. 9) shows a hilly topography with variations of about 250 ms TWT (*c*. 225 m) from low to high areas. The topography appears as a series of ridges elongated in a north-west – south-east direction, which probably represents folding introduced by superimposed sequential deformation over hanging-wall anticline crests and small extensional basins in the LTFL. The bumpy nature of the surface, especially in the east, is probably a combination of differential displacement across thrust faults in the LTFL and uncertainties in picking the reflection of the upper décollement surface, as this is not a clear and unambiguous reflection in all places (e.g. see Fig. 3, S.P. 0–350).

At the location of both SF1 and SF2, a hill-hole pair is outlined in the upper décollement surface (Fig. 9). The glaciotectonic feature referred to as hill-hole pair is applied in the sense of Aber *et al*. (1989).

A low-lying, elongated area striking west-south-west – east-north-east is situated between the two hill-hole pairs (Fig. 9). A tentative interpretation of this area could include a tear fault departing the two structures, SF1 and SF2. However, as SF1 and SF2 have different internal architectures, it is not a tear fault in the traditional sense, where the same structure can be found on each side of the tear fault (Hills 1963). However, in a glaciodynamic setting, the two structures could have undergone further deformation individually after the separation. The low-lying area shows a complex reflection pattern; hence, the seismic interpretation here is uncertain, probably due to the limitations of the seismic method and the complexity of the structure (e.g. Fig. 5, S.P. 1400–1500).

4.7. The structural trends in the UTFL

The structural trends of the thrust faults in UTFL are mapped to see if there were any discrepancies between the structural trends of UTFL, ITFL and LTFL, which could imply stress from different directions (Fig. 10). The thrust front to the west ends at the same location for the UTFL and the LTFL (Fig. 10). In general, the trends of the structures in UTFL are notably like those of the LTFL and ITFL, except for small discrepancies (Fig. 10), indicating that they have been subject to similar stresses during formation.

The structures of UTFL can be divided into two structural domains based on Fig. 3, a westerly distal domain, where imbricate thrust structures are translocated along the upper décollement surface until the eastern margin of SF1 (Fig. 3, S.P. 730–1260), and an easterly proximal domain, where the sediments are strongly deformed (see Fig. 3, S.P. 0–730). The thrusting of UTFL continues south of the study area, where LTFL is not deformed (Fig. 5, S.P. 550–880). The seismic lines in this area are, however, so far apart that the individual faults cannot be traced. Strike sections in the study area show large (up to *c*. 4–6 km) folded thrust sheets of UTFL in connection with and in between SF1 and SF2 (Fig. 5, S.P. 1200–1600 and Fig. 6, S.P. 2260–1875).

4.8. Restoration of the deformed sections

The method for performing the restoration is described in Section 3.3. The method is only giving a rough estimate of the minimum shortening across the two structural frameworks SF1 and SF2.

Figure 11 shows the restored section across SF1 from S.P. 550–1100 (Fig. 3). The restoration shows a minimum average shortening of UTFL of 44%, corresponding to a lateral displacement of 3400 m and only 9% average shortening of LTFL, corresponding to a lateral displacement of 600 m. The shortening of UTFL across SF1 is very strong with large displacements across each thrust fault. The displacement is generally much less in the LTFL, where extension at some points is the prevailing deformation (Step 3). Hence, the UTFL shows more compression than LTFL in the cross-section across SF1.

Figure 12 represents the restoration of a section across SF2 in the mid-north of the study area from S.P. 0–440 (Fig. 4). In this cross-section, the LTFL is repeated in an imbrication fan above the normal level of LTFL. The UTFL is forming a duplex stack in front of the imbrication

fan (Step 3 and Step 4 in Fig. 12). The average minimum shortening of the UTFL is 49% at SF2, corresponding to a lateral displacement of *c*. 2.2 km. The shortening of LTFL is 43%, corresponding to a lateral displacement of *c*. 3.8 km.

The restoration shows the amount of shortening in each thrust-fault level varies from place to place within the thrust-fault complex. Data from the fringing areas of the study area show that the deformation continues farther east of the mapped area, towards the coast. Therefore, a full account of shortening of the Fanø Bugt Glaciotectonic Complex cannot be provided with the existing data.

4.9. The structural framework and dynamic development of SF1 and SF2

The structural framework of SF1 is situated in the distal domain, although it has many similarities with the structures in the LTFL intermediate domain (Fig. 3). They both involve extensional faulting and have a frontal-thrust ramp with a low dip (Fig. 3). However, the strike of the faulting is like the strike of the structures of the distal domain (Fig. 8). The sequential development of SF1 comprises three dynamic phases illustrated in four steps in Fig. 11. Fault blocks in the LTFL are coloured green and annotated $SF1_1$–$SF1_4$. The normal fault imbricates (the extensional area) are grouped in $SF1_3$. The fault blocks in the UTFL are not annotated but coloured purple (Fig. 11). The four steps are described as follows:

1. **Step 1** (Fig. 11) presents the balanced cross-section of SF1, where the thrust sheets are organised into their pre-deformation position.
2. **Step 2** (Fig. 11) illustrates the first phase of initial deformation, where the UTFL is laterally displaced about 2.15 km, corresponding to 28% over the upper décollement surface, and the LTFL is compressed by 6% along the basal décollement surface. At the tailing end of the UTFL, a thrust-fault imbricate fan formed, which corresponds to the 2.15 km contraction. Note that the deformation of UTFL occurred slightly ahead of thrusting in LTFL.
3. **Step 3** (Fig. 11) illustrates the second phase, during which a hole is formed in the LTFL, and a piggyback imbricate fan of UTFL thrust sheets is piled up in the hole. A tentative interpretation is that body forces from the weight of the UTFL imbricate fan cause hydrodynamic shear deformation and the extensional normal fault imbricate fan in the LTFL ($SF1_3$ in Fig. 11). The fault block subject to hydrodynamic

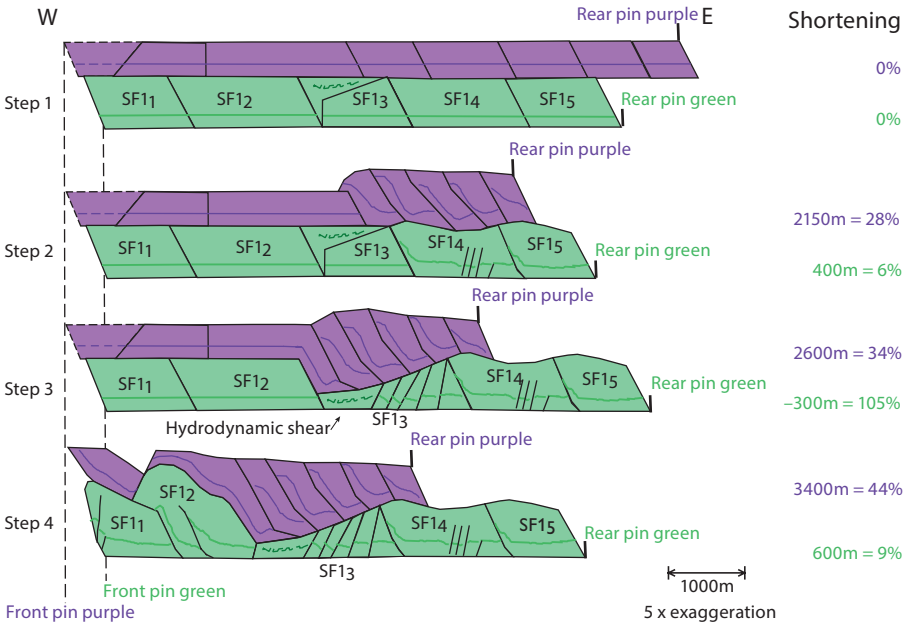

Fig. 11 Four steps in the dynamic development of the glaciotectonic framework SF1 illustrated by balancing and stepwise deformation of the segment S.P. 550–1100 of the seismic section in Fig. 3. Purple UTFL above green LTFL. To calculate the shortening, a fixed pin line is drawn at the front of each thrust-fault level and a loose pin in the rear. **Step 1** shows the balanced cross-section. The thrust sheets in LTFL are annotated $SF1_1$–$SF1_5$. **Step 2** shows initial translation of imbricate thrust faulting in both UTFL and LTFL. The thrusting of UTFL is slightly ahead of the thrusting in the LTFL. In **Step 3**, the weight of the imbricates in the UTFL created a combined hydrodynamic shear deformation and extensional normal fault imbricate with extension about 300 m, see $SF1_3$ in the LTFL. In **Step 4**, compressional thrust fault imbrication of the UTFL resulted in an imbricate fan. The fan filled the extensional depression and pushed $SF1_2$ above the leading thrust sheet $SF1_1$ forming a huge hanging wall anticline. The further compression of the LTFL proximal to the depression leads to normal faulting in UTFL above $SF1_2$. The total compression of this part of the section leads to a shortening of about 3400 m (44%) in the UTFL and 600m (9%) in LTFL (see also description in Sections 3.3, 4.8 and 4.9).

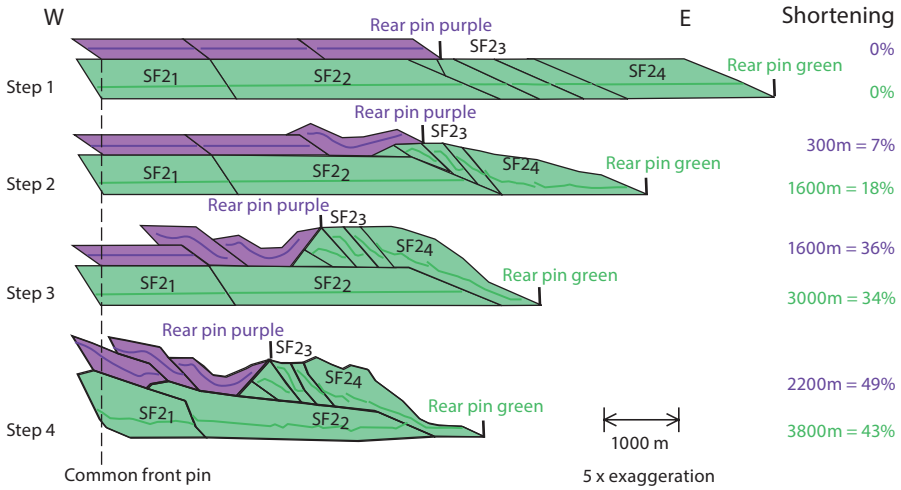

Fig. 12 Four steps in the dynamic development of the glaciotectonic framework SF2 illustrated by balancing and stepwise deformation of the segment S.P. 0–440 of the seismic section in Fig. 4. Purple UTFL above green LTFL. To calculate the shortening, a common fixed pin line is drawn at the front of the thrust-fault level and a loose pin in the rear of each level. **Step 1** shows the balanced cross-section. The thrust sheets in LTFL are annotated $SF2_1$–$SF2_4$. $SF2_3$ consists of the imbricate fan ITFL (Fig. 4). Small-scale deformation and hydrodynamically brecciated in the succession above and behind $SF2_3$ and $SF2_4$ (Fig. 4) are excluded from the reconstruction. **Step 2** shows the initial ramp collapse at the rear end of $SF2_2$ and imbrication of LTFL and gentle folding and displacement of UTFL above LTFL. In **Step 3**, the imbricate fan ($SF2_3$) starts to translate the tailing end of $SF2_2$. Piggyback on LTFL, the UTFL initiated to form a thrust-fault duplex stack above $SF2_2$. In **Step 4**, the duplex stack of UTFL is pushed by the translated imbricate fan $SF2_3$ on the thrust sheet back of $SF2_2$, and the tailing thrust sheet of UTFL is trapped in the position between the translated imbricate fan $SF2_3$ and the duplex stack of UTFL displaced towards the foreland. Compression is about 2200 m (49%) in the UTFL and 3800 m (43%) in the LTFL (see also description in Sections 3.3, 4.8 and 4.9).

shear is seen on the seismic sections as a non-reflective area (Fig. 3, S.P. 920–850). During this stage, the extension of LTFL was 5% greater than the compression.

4. **Step 4** (Fig. 11) illustrates the final phase, when the excessive weight of the UTFL in the hole caused more compression in front, pushing the huge thrust sheet of the LTFL ($SF1_2$ in Fig. 11). This generated a hanging wall anticline above $SF1_1$ and at the same time caused an even greater hole for the piggyback imbricate fan of the UTFL to slide into. This movement caused the observed hill-hole pair on the upper décollement surface (Fig. 9). Hence, it is suggested that body forces from the imbricate fan in UTFL were an important factor in the formation of SF1. The resulting compression of the UTFL and LTFL is *c*. 44% and *c*. 9%, respectively.

The structural framework for SF2 is situated in the intermediate domain of LTFL in the northern part of the investigated area (Fig. 4, S.P. 0–250; Fig. 8). The north-eastern part of the structure could not be fully mapped because the linespacing is too large (Figs 1, 8). SF2 consists of an imbricate fan, which, as a whole segment, was translated up along an easterly dipping ramp and displaced across a flat (the intermediate décollement in Fig. 4). The top of SF2 is truncated by a roof thrust (the upper décollement). The sequential evolution of SF2 can be divided into four phases, as illustrated in the four steps in Fig. 12. These four steps are described as follows:

1. **Step 1** (Fig. 12) illustrates the balanced cross-section of the segment between S.P. 0–440 from Fig. 4. The thrust sheets in the LTFL are annotated $SF2_1$–$SF2_4$. Note that the succession with a chaotic reflection pattern above and behind the ITFL is excluded from the reconstruction (Fig. 4).
2. **Step 2** (Fig. 12) illustrates the early phase of deformation, where the ramp collapses, and imbrication of thrust sheets in the LTFL is initiated. Internal deformation of $SF2_4$ is happening, and compression of the thrust sheet $SF2_3$ results in an imbricate fan. Moreover, gentle folding and displacement of thrust sheets in UTFL start.
3. **Step 3** (Fig. 12). In this phase, the thrust sheets constituting the imbricate fan ($SF2_3$) are pushed farther up the ramp by thrust sheet $SF2_4$ and translated piggyback on top of the LTFL towards the foreland. In front of the imbricate fan ($SF2_3$), UTFL started to form a thrust-fault duplex stack.
4. **Step 4** (Fig. 12). In the final phase, the translation of the imbricate fan ($SF2_3$) continues. A combination of uplift and push from the rear resulted in the further development of the duplex stack of the UTFL, which is carried piggyback on top of thrust sheets $SF2_1$ and $SF2_2$. In this final phase, the tailing thrust sheet of UTFL became trapped in the position between the translated imbricate fan of the LTFL ($SF2_3$) and the duplex stack of UTFL. The frontal part of the duplex stack was thrust up and displaced towards the

foreland, and minor ramp thrusting of the frontal part of $SF2_2$ accentuated the central depression above the UTFL developed in SF2.

5. Discussion

This study shows that the investigated part of the Fanø Bugt Glaciotectonic Complex consists of large-scale thrust fault structures on the scale of hundreds of metres to kilometres. The structures constitute a duplex in two thrust fault levels separated by an internal décollement surface. The basal décollement surface is weakly inclined (around 0.5°) towards the direction of transport of thrust faults. The age of the deformed sediments ranges from lower Miocene and younger sediments with a thin Quaternary sediment covering above an erosional surface mapped in Larsen & Andersen (2004). Inside the complex, different structural styles are recognised, and in several places, normal faulting occurs, resulting in extension in an otherwise compressional setting.

5.1. Unique features of the Fanø Bugt Glaciotectonic Complex

Although glaciotectonic complexes have been described in many studies from all over the world, only a few were discovered on a scale comparable to the Fanø Bugt Glaciotectonic Complex (e.g. Pedersen & Boldreel 2015, 2017; Winsemann *et al.* 2020; Lohrberg *et al.* 2022). Common amongst those glaciotectonic complexes is that they all involve Pre-Quaternary sediments. This is possibly because Pre-Quaternary sediments often by their nature are more compressed than Quaternary sediments and, therefore, have greater coherence, hence the ability to evolve larger coherent thrust sheets than seen in studies only involving Quaternary sediments (e.g. Vaughan-Hirsch & Phillips 2017; Phillips *et al.* 2018).

The Heligoland Glaciotectonic Complex in the German sector is less than 100 km south of Fanø Bugt Glaciotectonic Complex and is the most comparable, described by Lohrberg *et al.* (2022). The Heligoland Glaciotectonic Complex is comparable in scale and has many similar structural features, such as imbrications in two levels separated by an internal décollement surface, a detail, which is seldom described for glaciotectonic complexes. Analogues in terms of their orogenic setting with multiple detachment levels and imbrications in two levels have been described for the central Andes of Peru, the Norwegian Caledonides and the Cumberland Plateau in the Southern Appalachians (Pfiffner 2017).

A basal décollement surface dipping towards the transport direction of the thrust faults and the ice sheet, as seen in the Fanø Bugt Glaciotectonic Complex, is also found at the Heligoland Glaciotectonic Complex (Lohrberg *et al.* 2022) and in other glaciotectonic complexes in the eastern part of the North Sea (Huuse & Lykke-Andersen 2000a). The basal décollement of the Fanø Bugt Glaciotectonic Complex is situated in lower Miocene sediments and has a maximum depth of 400 ms TWT. The basal décollement of the Heligoland Complex is situated a bit higher (350 ms TWT) and at a younger stratigraphic level, the Miocene-Pliocene boundary (Lohrberg *et al.* 2022). The glaciotectonic complexes situated north of Fanø Bugt have décollements at the Mid Miocene unconformity or at the Base Quaternary boundary at a depth of 150–300 ms TWT (Huuse & Lykke-Andersen 2000a).

Three zones of deformation are identified in both the Heligoland Glaciotectonic Complex (Lohrberg *et al.* 2022) and the Fanø Bugt Glaciotectonic Complex. However, while the Heligoland Glaciotectonic Complex shows the steepest thrust angles close to the ice margin in the hinterland, like ones observed in other glaciotectonic complexes (e.g. Pedersen 2005; Phillips *et al.* 2017), the opposite pattern is observed in the LTFL in the Fanø Bugt Glaciotectonic Complex. Here, thrust faults steepen towards the foreland (Fig. 3, no exaggeration section), deviating from the typical pattern observed in fold and thrust deformation.

The average shortening found in this study varies from 9 to 49% (Figs 11 and 12). It was measured not only across parts of the complex that potentially experienced the largest compression but also in the area of largest extension (LTFL in SF1, step 3; Figs 3–6, 8). Hence, it only resembles the shortening in the part of the complex where the two profiles exist and does not represent the total shortening of the Fanø Bugt Glaciotectonic Complex.

This study shows that the LTFL has experienced much less compression in certain areas than the UTFL and also less compression when compared to glaciotectonic complexes in general, 11–61% (values from Croot 1988; Hart 1990, 1994, 1995; Klint & Pedersen 1995; Pedersen 1996, 2005, 2014; Harris *et al*. 1997; Boulton *et al.* 1999; Huuse & Lykke-Andersen 2000a; Williams *et al*. 2001; Gehrmann 2019; Winsemann *et al*. 2020; Lohberg *et al.* 2022; Vaughan *et al*. 2024). This is most likely due to the relatively large amount of extension found in the LTFL in certain areas of the Fanø Bugt Glaciotectonic Complex. Furthermore, the limitations of the seismic data in resolving small-scale or very steeply inclined structures will result in a minimum calculation of the compression, when compared to studies on seismic data with a higher resolution or studies of onshore outcrops where small-scale details can be included in the restoration of the glaciotectonic complexes.

We attribute the unique features of the Fanø Bugt Thrust Complex (highlighted here) to the deformation

mechanism. Thus, there may have been a subtle interaction between various features that could facilitate deformation during the formation of the complex.

5.2. Deformation mechanisms and structural styles

In the Fanø Bugt Glaciotectonic Complex, different deformation domains exist, each characterised by various types of structures, a common phenomenon in thin-skinned tectonics both in orogenic settings and glacial settings (e.g. Boulton *et al.* 1999; Pedersen & Boldreel 2015). Various structural styles occur in the individual thrust fault levels, which may be related to the former position of the ice-sheet margin responsible for the deformation. Glaciotectonic deformation is generally considered to be driven by a gravity-spreading mechanism (e.g. van der Wateren 1985; Pedersen 1987; Aber *et al*. 1989; Andersen *et al.* 2005); however, it could also be argued that some of the structures found in this study indicate a gravity-gliding mechanism contributed to the deformation.

The UTFL can be divided into two different structural domains based on the different structural styles: (1) a distal domain showing thrusting and folding implying proglacial deformation; (2) a proximal domain showing a chaotic reflection pattern, interpreted to resemble pervasively sheared or chaotically mixed sediments (Aber 1985), boudinage structures (Berthelsen 1979), fluid flow structures and hydrodynamic brecciation (Pedersen 2005). These structures imply subglacial deformation or a combination of both proglacial and a later phase of subglacial deformation.

The reflection pattern of the strongly sheared and deformed sediments of the UTFL stops abruptly at the upper décollement surface (Fig. 3, UTFL, proximal domain). Hence, it is suggested that the upper décollement surface absorbs the induced subglacial stress and prevents the same kind of deformation of the sediments below this surface. An exception is seen in the easternmost part of the study area, where the entire sediment package down to the basal décollement surface was probably subject to strong subglacial deformation (Fig. 3, LTFL, S.P. 0–125).

The LTFL exhibits three structural domains with different structural styles, which changes in dip (Fig. 3) and strike (Fig. 8) of the faults along the direction of transport. The structural styles mostly imply proglacial deformation, except for the presence of extensional faulting, mainly in the intermediate domain (Fig. 3), and the pervasively sheared or chaotically mixed sediments in the easternmost end of the proximal domain (Fig. 3). The structural frameworks in the intermediate domain comprise a combination of compressional and extensional faulting, which may imply subglacial deformation close to the ice margin (Croot 1987). Hence, each framework may reflect the position of the ice margin. If this is the case, subglacial stress did go deeper than the upper décollement. However, the excessive load of the UTFL piggyback imbricates in the hole of SF1 could also have induced the hydrodynamic shear and extension, as seen in the LTFL ($SF1_3$, step 3, Fig. 11).

Extensional faulting in glaciotectonic settings has been described in a few studies (Croot 1988; Pedersen 2005; Vaughan *et al*. 2024). However, the existence of several structural frameworks of thrust faults with tailing listric normal faults detaching on a gently dipping basal décollement surface (Fig. 3, intermediate domain of LTFL) has, to our knowledge, not previously been reported in glaciotectonic settings. This structural framework has, although on a much smaller scale, huge similarities with structural frameworks seen in deep-water thrust fault belts (DWTFB; e.g. Morley *et al*. 2011; Mahanjane & Franke 2014), where a linkage of up-dip extension with down-dip contraction via a dipping detachment zone is usually associated with the mechanism of gravity gliding (Morley *et al*. 2011).

This combination of structural styles and deformation types seems to be unique for the Fanø Bugt Glaciotectonic Complex, compared with other large-scale glaciotectonic complexes. One hypothesis is that the deformation mechanism was gravity spreading caused by the load of an ice sheet, and in the case of SF1 helped by the excessive body mass of a piggyback imbricate fan in the UTFL, combined with the mechanism of gravity gliding due to the inclined basal décollement surface.

The basal décollement surface in the Fanø Bugt Glaciotectonic Complex is a gently inclined surface situated in Lower Miocene sediments with an approximate dip of 0.5° (Andersen 2004). A distinct change in strike and dip of the basal décollement surface occurs on each side of the study area (Fig. 7). Hence, the area stands out as having a lower inclination than the surrounding areas and a dip in the main part of the area parallel to the direction of transport of the LTFL. This begs the question as to whether this variation in dip of the décollement surface could have influenced the deformation. One hypothesis is that porewater flowing from the north was directed towards the study area following the dip of the basal décollement surface. The decrease in dip and change in strike on the border of the study area (Fig. 7) would slow porewater flow, allowing porewater pressure to build up. The high porewater pressure could have facilitated deformation and enhanced the possibility of both gravity spreading and gravity gliding.

The Fanø Bugt Glaciotectonic Complex was formed by an ice sheet coming from an eastern source area (Huuse & Lykke-Andersen 2000a; Andersen 2004). The

coincidence in the dip direction of the basal décollement surface and transport direction of the ice sheet possibly enhanced the deformation forces and caused the deformation to reach its maximum extent in the area studied here compared to the rest of the Fanø Bugt Glaciotectonic Complex, note the curvature on the deformation front (Fig. 7).

The dipping décollement towards the foreland in the Fanø Bugt Complex contrasts with the common critical taper wedge models, where the basal detachment dips in the opposite direction towards the hinterland (Davis *et al.* 1983). However, it is important to keep in mind that it is the direction of dip of the topographic surface that drives the thrust movement and not the dip of the décollement (van der Pluijm & Marshak 2004). In the case of a glaciotectonic complex, the topographic surface of the ice provides the driving mechanism (Aber *et al.* 1989; Andersen *et al*. 2005). In the case of the Fanø Bugt Glaciotectonic Complex, a relatively huge topographic high must have developed in connection with the formation of SF2, where the green reflection is elevated about 150 ms (*c.* 140 m) above normal level (Fig. 4). However, this raised topography is concentrated in a relatively small area (Fig. 8).

5.3. The kinematics of the Fanø Bugt Glaciotectonic Complex

The kinematic evolution of the two structural frameworks SF1 and SF2 shows that the deformation of the UTFL preceded that of the LTFL (Figs 11 and 12). This is supported by the map of the internal décollement (Fig. 9), which shows a wavy pattern with highs above thrust ridges and lows in between, indicating superimposed deformation. This should be seen in contrast to the area south of the study area, where the UTFL is sliding on a planar décollement surface, and no LTFL exists (Figs 5 and 6).

Based on our observations, we suggest that progressive deformation took place nearly simultaneously, in the LTFL and UTFL, but with a small difference in timing during propagation from the east to west.

The deformations reach their maximum depth in the south-western corner of the study area, approximately coinciding with the 400 ms TWT (*c*. 360 m) contour curve of the basal décollement (Fig. 7). This may indicate that the south-western limit of the deformation of the LTFL in the Fanø Bugt Glaciotectonic Complex was controlled by the depth to the basal décollement (Andersen 2004; Andersen *et al*. 2005). The deformation of the UTFL continues farther to the south beyond the study area (Figs 5 and 6).

The westward progression of the deformation front is located at the same position for both the UTFL and the LTFL (Figs 3, 4, 10), suggesting that the deformation at both levels occurred during the same deformation event. This conclusion was also drawn in the case of the Heligoland Glaciotectonic Complex (Lohrman *et al.* 2022), where similar thrust fault architecture is observed. A key argument, which applies to both the Heligoland and Fanø Bugt Glaciotectonic Complexes, is the absence of undisturbed sediments and erosional truncation between the two levels of deformation. This suggests that the folds and thrusts at both levels formed contemporaneously, likely as part of a single deformational event.

6. Conclusions

The mapped area of the Fanø Bugt Glaciotectonic Complex contributes significant documentation of large-scale glaciodynamic features in the south-eastern North Sea. The complex architecture includes two main thrust-fault levels (LTFL and UTFL) and possibly a third (ITFL) in a small area. The LTFL is a duplex comprising imbricate thrust sheets and normal faults, detaching on a westward dipping basal décollement surface. The roof thrust of the duplex acts as an internal décollement, separating imbricated thrust faults of the UTFL from the LTFL. Thrust ridges range from hundreds of metres to kilometres scale, with crest elevation varying from a few tens of metres to more than 150 m above the level of the foreland deposits. Deformation extends down to *c*. 400 ms TWT at *c*. 360 m b.s.l., and prominent hanging-wall ridges can be traced along strike for more than *c*. 10 km.

The UTFL reflects sequential superimposed deformation of the LTFL, both presumably formed during the same pre-Weichselian ice advance from the east. The deformation propagated westward with slight temporal offsets between the LTFL and the UTFL and a varying shortening within the complex.

Structural styles vary across the complex, from east to west, as do the strike and dip of the faults. The UTFL generally deforms in a more ductile way than the LTFL, due to differences in sediment rheology. The LTFL represents the Early/Middle Miocene marine Arnum Formation with possible intercalations of the sandy Bastrup and Odderup Formations, whereas the UTFL constitutes the Middle Miocene, fully marine clayey Hodde and Gram Formations.

Two spectacular structural frameworks, SF1 and SF2, have been analysed. Both structures include a hidden hill-hole pair potentially separated by a tear fault. A tentative restoration of profiles across SF1 and SF2 shows an average minimum shortening of *c*. 9–43% of the LTFL and *c*. 44–49% of the UTFL. The displacement varied in the order of –300 m (extension) and up to 3.8 km (compression).

The unique combination of architecture and structural styles suggests a deformation mechanism involving

a combination of proglacial gravity spreading caused by the differential load of the ice sheet, possibly aided by gravity gliding due to the inclined basal décollement surface. High porewater pressure and the alignment of ice-sheet movement with the basal décollement dip possibly facilitated deformation further.

If an opportunity arises to collect core material from within the complex, it would be valuable for future research to enable detailed analyses of the physical and mechanical properties of the sediments in and around the décollement surfaces and thereby enhance our understanding of the mechanism behind their formation. Core material could also help constrain the glaciostratigraphic timing of the complex. Furthermore, seismic data with a higher resolution could contribute with images of smaller-scale structures, distinct sedimentary units and more accurate erosional contacts within the top 50–100 ms TWT, hence provide better conditions for reconstructing a detailed history of ice advance.

Acknowledgements

Holger Lykke-Andersen, Peter R. Jakobsen and James A. Chalmers are thanked for valuable discussions and comments on a first draft of the manuscript. Kristian A. Rasmussen and Anders Mathisen are thanked for the help with the topographic subsurface maps and Jette Halskov for the help with refinement of figures. The authors would like to thank David Collin Tanner and an anonymous reviewer for providing critical comments and suggestions that greatly improved the manuscript.

Additional information

Funding statement

This project was financed by the Geological Survey of Denmark and Greenland and the Danish Research Agency. The seismic data were financed by The Royal Danish Administration of Navigation and Hydrography, the Geological Survey of Denmark and Greenland and the University of Aarhus. The Royal Danish Navy provided the ship for acquisition.

Author contributions

LTA: Conceptualisation, interpretation of seismic data, writing original draft, structural analysis, visualisation.
SASP: Conceptualisation, interpretation, structural analysis.

Competing interests

The authors declare no competing interests.

Data availability statement

None provided.

References

Aber, J.S. 1985: The character of glaciotectonism. Geologie en Mijnbouw **64**, 389–395.

Aber, J.S. & Ber, A. 2007: Glaciotectonism. Developments in Quaternary Sciences **6**, 246 pp.

Aber, J.S., Croot, D. & Fenton, M.M. 1989: Glaciotectonic landforms and structures. Glaciology and Quaternary Geology series, 200 pp. Kluwer Academic Publishers, Dordrecht. *https://doi.org/10.1007/978-94-015-6841-8_10*

Andersen, L.T. 2004: The Fanø Bugt Glaciotectonic Thrust Fault Complex, Southeastern Danish North Sea. A study of large-scale glaciotectonics using high-resolution seismic data and numerical modelling. Danmarks og Grønlands Geologiske Undersøgelse Rapport **30**, 143 pp. PhD thesis, University of Aarhus.

Andersen, L.T., Hansen, D.L. & Huuse, M. 2005: Numerical modelling of thrust structures in unconsolidated sediments: implications for glaciotectonic deformation. Journal of Structural Geology **27**, 587–596. *https://doi.org/10.1016/j.jsg.2005.01.005*

Andersen, T.R., Poulsen, S.E, Christensen, S. & Jørgensen, F. 2013: A synthetic study of geophysics–based modelling of groundwater flow in catchments with a buried valley. Hydrogeology Journal **21**, 491–503. *https://doi.org/10.1007/s10040-012-0924-5*

Berthelsen, A. 1979: Recumbent folds and boudinage structures formed by subglacial shear, an example of gravity tectonics. In: van der Linden, W.J.M. (ed.): Fixism, mobilism or relativism: Van Bemmelens Search, 253–260.

Berthelsen, F. & Kristoffersen, N.F. 1974: On the environments and stratigraphy of the Late Tertiary of Rømø, SW Denmark. Danmarks Geologiske Undersøgelse, Årbog **1973**, 5–14, Danmarks Geologiske Undersøgelse, Copenhagen.

Boulton, G.S. & Caban, P. 1995: Groundwater flow beneath ice sheets: Part **II** – Its impact on glacier tectonic structures and moraine deformation. Quaternary Science Reviews **14**, 563–587. *https://doi.org/10.1016/0277-3791(95)00058-w*

Boulton, G.S., van der Meer, J.J.M., Beets, D.J., Hart, J.K. & Ruegg, G.H.J. 1999: The sedimentary and structural evolution of a recent push moraine complex: Holmstrømsbreen, Spitsbergen. Quaternary Science Reviews **18**, 339–371. *https://doi.org/10.1016/s1571-0866(04)80103-9*

Boyer, S.E. & Elliott, D. 1982: Thrust Systems. AAPG Bulletin **66**, 1196–1230. *https://doi.org/10.1306/03b5a77d-16d1-11d7-8645000102c1865d*

Brandes, C. & Le Heron, D.P. 2010: The glaciotectonic deformation of Quaternary sediments by fault-propagation folding. Proceedings of the Geologists' Association **121**, 270–280. *https://doi.org/10.1016/j.pgeola.2010.03.001*

Burke, H., Phillips, E., Lee, J.R. & Wilkinson, I.P. 2009: Imbricate thrust stack model for the formation of glaciotectonic rafts: an example from the Middle Pleistocene of north Norfolk, UK. Boreas **38**, 620–637. *https://doi.org/10.1111/j.1502-3885.2009.00085.x*

Butler, R.W.H. 1987: Thrust sequences. Journal of the Geological Society of London **144**, 619–634. *https://doi.org/10.1144/gsjgs.144.4.0619*

Clausen, O.R. & Huuse, M. 1999: Topography of the Top Chalk Surface on and offshore Denmark. Marine and Petroleum Geology **16**, 677–691. *https://doi.org/10.1016/s0264-8172(99)00003-3*

Croot, D.G. 1987: Glacio-tectonic structures: A mesoscale model of thin-skinned thrust sheets? Journal of Structural Geology **9**, 797–808. *https://doi.org/10.1016/0191-8141(87)90081-2*

Croot, D.G. 1988: Morphological, structural and mechanical analysis of neoglacial ice-pushed ridges in Iceland. In: Croot, D.G. (ed.): Glaciotectonics: Forms and Processes, 33–48. Balkema, Rotterdam.

Dahlstrom, C.D.A. 1969: Balanced cross-sections. Canadian Journal of Earth Sciences **6**, 743–757. *https://doi.org/10.1139/e69-069*

De Paor, D.G. 1988: Balanced section in thrust belts part 1: construction. AAPG Bulletin **72**(1), 73–90. *https://doi.org/10.1306/703c81cd-1707-11d7-8645000102c1865d*

Ehlers, J. 1990: Reconstructing the dynamics of the North-West European Pleistocene ice sheets. Quaternary Science Reviews **9**, 71–83. *https://doi.org/10.1016/0277-3791(90)90005-u*

Friis, H. 1995: Neogene aflejringer. In: Nielsen, O.B. (ed.): Danmarks geologi fra Kridt til i dag. Aarhus Geokompendier **1**, 115–128. Aarhus Geokompendier Aarhus University, Aarhus.

Gehrmann, A., Meschede, M., Hüneke, H. & Pedersen, S.A.S. 2019: Sea cliff at Kieler Ufer (Pleistocene stripes 11–16) – Large-scale architecture and kinematics of the Jasmund Glacitectonic Complex. DEUQUA Special Publications **2**, 19–27. *https://doi.org/10.5194/deuquasp-2-19-2019*

Harris, C., Williams, G., Bramham, P., Eaton, G. & McCarroll, D. 1997: Glaciotectoniczed Quaternary sediments at Dinas Dinille, Gwynedd, North Wales, and their bearing on the style of deglaciation in the Eastern Irish Sea. Quaternary Science Reviews **16**, 109–127. *https://doi.org/10.1016/s0277-3791(96)00050-9*

Hart, J.K. 1990: Proglacial glaciotectonic deformation and the origin of the Cromer Ridge push moraine complex, North Norfolk, England. Boreas **19**, 165–180. *https://doi.org/10.1111/j.1502-3885.1990.tb00577.x*

Hart, J.K. 1994: Proglacial glaciotectonic deformation at Melabakkar-Ásbakkar, west Iceland. Boreas **23**, 112–121. *https://doi.org/10.1111/j.1502-3885.1994.tb00592.x*

Hart, J.K. 1995: Drumlin formation in Southern Anglesey and Arvon, Northwest Wales. Journal of Quaternary Science **10**, 3–14. *https://doi.org/10.1002/jqs.3390100103*

Hart, J.K. & Boulton, G.S. 1991: The interrelation of glaciotectonic and glaciodepositional processes within the glacial environment. Quaternary Science Reviews **10**, 335–350. *https://doi.org/10.1016/0277-3791(91)90035-s*

Hills, E.S. 1963: Elements of structural geology. New York: Wiley, 483 pp. *https://doi.org/10.4324/9781003465362*

Hossack, R.J. 1979: The use of balanced cross-sections in the calculation of orogenic contraction: A review. Journal of the Geological Society **136**, 705–711. *https://doi.org/10.1144/gsjgs.136.6.0705*

Houmark-Nielsen, M. 2007: Extent and age of Middle and late Pleistocene glaciations and periglacial episodes in southern Jylland, Denmark. Bulletin of the Geological Society of Denmark **55**, 9–35. *https://doi.org/10.37570/bgsd-2007-55-02*

Houmark-Nielsen, M. 2011: Pleistocene glaciations in Denmark: a closer look at chronology, ice dynamics and landforms. In: Ehlers, I. *et al.* (eds): Quaternary glaciations – Extent and chronology. Developments in Quaternary Science **2**, 47–57. Elsevier, Amsterdam. *https://doi.org/10.1016/b978-0-444-53447-7.00005-2*

Hubbert, M.K. & Ruby, W.W. 1959: Role of fluid pressure in mechanics of overthrust faulting. Geological Society of America Bulletin **70**, 115–166. *https://doi.org/10.1130/0016-7606(1959)70[167:rofpim]2.0.co;2*

Huuse, M. 2000: Cenozoic evolution of the eastern North Sea Basin – New evidence from high-resolution and conventional seismic data. 130 pp. PhD Thesis, Aarhus Geoscience.

Huuse, M. 2002: Late Cenozoic palaeogeography of the eastern North Sea Basin: climatic vs. tectonic forcing of basin margin uplift and deltaic progradation. Bulletin of the Geological Society of Denmark **49**, 145–169. *https://doi.org/10.37570/bgsd-2003-49-12*

Huuse, M. & Lykke-Andersen, H. 2000a: Large-scale glaciotectonic thrust structures in the eastern Danish North Sea. In: Maltman, A. *et al.*: Deformation of Glacial Materials. Geological Society, London, Special Publications **176**, 293–305. *https://doi.org/10.1144/gsl.sp.2000.176.01.22*

Huuse, M. & Lykke-Andersen, H. 2000b: Overdeepened Quaternary valleys in the eastern Danish North Sea: morphology and origin. Quaternary Science Reviews **19**, 1233–1253. *https://doi.org/10.1016/S0277-3791(99)00103-1*

Huuse, M., Lykke-Andersen, H. & Michelsen, O. 2001: Cenozoic evolution of the eastern Danish North Sea. Marine Geology **177**, 243–269. *https://doi.org/10.1016/s0025-3227(01)00168-2*

Høyer, A.S., Jørgensen, F., Piotrowski, J.A. & Jakobsen, P.R. 2013: Deeply rooted glaciotectonism in western Denmark: geological composition, structural characteristics and the origin of Varde hill-island. Journal of Quaternary Science **28**(7), 683–696. *https://doi.org/10.1002/jqs.2667*

Japsen, P. 1998: Regional Velocity-Depth Anomalies, North Sea Chalk: a record of overpressure and Neogene Uplift and Erosion. AAPG Bulletin **82**, 2031–2074. *https://doi.org/10.1306/00aa7bda-1730-11d7-8645000102c1865d*

Jordt, H., Faleide, J.I, Bjørlykke, K. & Ibrahim, M.T. 1995: Cenozoic sequence stratigraphy of the central and northern North Sea basin: tectonic development, sediment distribution and provenance areas. Marine Petroleum Geology **12**, 845–879. *https://doi.org/10.1016/0264-8172(95)98852-v*

Jørgensen, F. *et al.* 2012: Transboundary geophysical mapping of geological elements and salinity distribution critical for the assessment of future sea water intrusion in response to sea level rise. Hydrology and Earth System Sciences **16**, 1845–1862. *https://doi.org/10.5194/hess-16-1845-2012*

Klint, K.E.S. & Pedersen, S.A.S. 1995: The Hanklit glaciotectonic thrust fault complex, Mors, Denmark. Danmarks Geologiske Undersøgelse Serie A **35**, 30 pp. *https://doi.org/10.34194/seriea.v35.7055*

Knudsen, K.L. & Penny, D.N. 1987: Foraminifera and Ostracoda in Late Elsterian-Holsteinian deposits at Tornskov and adjacent areas in Jutland, Denmark. Danmarks Geologiske Undersøgelse Serie B **10**, 7–67. *https://doi.org/10.34194/serieb.v10.7076*

Kupetz, M. 2001: Glazialtektonik Von der Wirkung pleistozäner Inlandeisgletcher, Naturwissenschaftliche Rundschau **54**, Jahrgang 9, Stuttgart, 457–464.

Larsen, B. & Andersen, L.T. 2005: Late Quaternary stratigraphy and morphogenesis in the Danish eastern North Sea and its relation to onshore geology. Netherlands Journal of Geosciences – Geologie en Mijnbouw **84**, 113–128. *https://doi.org/10.1017/s0016774600023003*

Lohrberg, A., Schwarzer, K., Unverricht, D., Omlin, A. & Krastel, S. 2020: Architecture of tunnel valleys in the southeastern North Sea: new insights from high-resolution seismic imaging. Journal of Quaternary Science **35**, 892–906. *https://doi.org/10.1002/jqs.3244*

Lohrberg, A., Krastel, S., Unverricht, D. & Schwarzer, K. 2022: The Heligoland Glacitectonic Complex In the southeastern North Sea: indicators of a pre- or early Elsterian ice margin. Boreas **51**, 100–117. *https://doi.org/10.1111/bor.12551*

Mahanjane, E.S. & Franke, D. 2014: The Rovuma Delta deep-water fold-and-thrust belt, offshore Mozambique. Tectonophysics **614**, 91–99. *https://doi.org/10.1016/j.tecto.2013.12.017*

Mathews, W.H. & Mackay, J.R. 1960: Deformation on soils by ice and the influence of porewater pressure on permafrost. Transactions of the Royal Society of Canada **54**, 27–36.

Michelsen, O., Thomsen, E., Danielsen, M., Heilmann-Clausen, C., Jordt, H. & Lauersen, G.V. 1999: Cenozoic sequence stratigraphy in the eastern North Sea. In: de Graciansky, P.Ch. *et al.* (eds.): Mesozoic and Cenozoic Sequence Stratigraphy of Western European Basins. Society of Sedimentary Geology (SEPM) Special Publication **60**, 91–118. SEPM (Society for Sedimentary Geology), Tulsa, Oklahoma. *https://doi.org/10.2110/pec.98.02.0091*

Moran, S.R. 1971: Glaciotectonic structures in Drift. In: Goldthwait, R.P. (ed.): Till, a symposium, 127–148. Columbus: Ohio State University Press.

Morley, C.K., King, R., Hillis, R., Tingay, M. & Backe, G. 2011: Deepwater fold and thrust belt classification, tectonics, structure and hydrocarbon prospectivity: a review. Earth-Science Reviews **104**(1–3), 41–91. *https://doi.org/10.1016/j.earscirev.2010.09.010*

Nielsen, L.H. & Japsen, P. 1991: Deep wells in Denmark 1935–1990. Lithostratigraphic subdivision. Geological Survey of Denmark. Danmarks Geologiske Undersøgelse Serie A **31**, 179 pp.

Ottesen, D., Steward, M., Brönner, M. & Batchelor, C.L. 2020: Tunnel valleys of the central and northern North Sea (56°N to 62°N): Distribution and characteristics. Marine Geology **425**, 1–19. *https://doi.org/10.1016/j.margeo.2020.106199*

Pedersen, S.A.S. 1987: Comparative studies of gravity tectonics in Quaternary sediments and sedimentary rocks related to fold belts. In: Jones, M.E. & Preston, R.M.F. (eds): Deformation of sediments and sedimentary rocks. Geological Society, London. Special Publications **29**, 165–180. *https://doi.org/10.1144/gsl.sp.1987.029.01.14*

Pedersen, S.A.S. 1996: Progressive glaciotectonic deformation in Weichselian and Palaeogene deposits at Feggeklit, Northern Denmark. Bulletin of the Geological Society of Denmark **42**, 153–174. *https://doi.org/10.37570/bgsd-1995-42-13*

Pedersen, S.A.S. 2000–02–10: Superimposed deformation in glaciotectonics, Bulletin of the Geological Society of Denmark **46**, 125–144. Copenhagen. *https://doi.org/10.37570/bgsd-1999-46-11*

Pedersen, S.A.S. 2005: Structural analysis of the Rubjerg Knude Glaciotectonic Complex. Vendsyssel, northern Denmark. Geological Survey of Denmark and Greenland Bulletin **8**, 192 pp + 2 plates. *https://doi.org/10.34194/geusb.v8.5253*

Pedersen, S.A.S. 2014: Architecture of Glaciotectonic Complexes. Geosciences **2014**(4), 269–296. *https://doi.org/10.3390/geosciences4040269*

Pedersen, S.A.S. & Boldreel, L.O. 2015: Thrust fault architecture of glaciotectonic complexes in Denmark. Geological Survey of Denmark and Greenland Bulletin **33**, 17–20. *https://doi.org/10.34194/geusb.v33.4479*

Pedersen, S.A.S. & Boldreel, L.O. 2017: Glaciotectonic deformations in the Jammerbugt and glaciodynamic development in the eastern North Sea. Journal of Quaternary Science **32**(2), 183–195. *https://doi.org/10.1002/jqs.2887*

Pfiffner, O.A. 2017: Thick-skinned and thin-skinned tectonics: A global perspective. Geosciences **7**, 71, 1–89. *https://doi.org/10.3390/geosciences7030071*

Phillips, E., Evans, D.J.A., Atkinson, N. & Kendall, A. 2017: Structural architecture and glacitectonic evolution of the Mud Buttes cupola hill complex, Southern Alberta, Canada. Quaternary Science Reviews **164**, 110–139. *https://doi.org/10.1016/j.quascirev.2017.03.027*

Phillips, E., Cotterill, C., Johnson, K., Crombie, K., James, L., Carr, S. & Ruiter, A. 2018: Large-scale glaciotectonic deformation in response to active ice sheet retreat across Dogger Bank (southern central North Sea) during the Last Glacial Maximum. Quaternary Science Reviews **179**, 24–47. *https://doi.org/10.1016/j.quascirev.2017.11.001*

Prins, L.T. & Andersen, K.J. 2019: Buried late Quaternary channel systems in the Danish North Sea –Genesis and geological evolution. Quaternary Science Reviews **223**, 105943. *https://doi.org/10.1016/j.quascirev.2019.105943*

Rasmussen, E.S. 1996: Sequence stratigraphic subdivision of the Oligocene and Miocene succession in South Jutland. Bulletin of the Geological Society of Denmark **43**, 143–155. *https://doi.org/10.37570/bgsd-1996-43-14*

Rasmussen, E.S. 2004: Stratigraphy and depositional evolution of the uppermost Oligocene – Miocene succession in Denmark. Bulletin of the Geological Society of Denmark **51**, 89–109. *https://doi.org/10.37570/bgsd-2004-51-07*

Rasmussen, E.S., Dybkjær, K. & Piasecki, S. 2010: Lithostratigraphy of the Upper Oligocene – Miocene succession of Denmark. Geological Survey of Denmark and Greenland Bulletin **22**, 92 pp. *https://doi.org/10.34194/geusb.v22.4733*

Rosenkrantz, A. 1944: Nye bidrag til Forståelsen af Ristinge Klints Opbygning. Dansk Geologisk Forening **10**, 431–435.

Salomonsen, I. 1995: Origin of a deep buried valley system in Pleistocene deposits of the eastern central North Sea. In: Michelsen, O. (ed.): Proceedings of the Second Symposium on Marine Geology – Geology of the North Sea and Skagerrak. Danmarks Geologiske Undersøgelse Serie C **12**, 7–19. Geological Survey of Denmark, Copenhagen. *https://doi.org/10.34194/seriec.v12.7106*

Sandersen, P.B.E. & Jørgensen, F. 2017: Buried tunnel valleys in Denmark and their impact on the geological architecture of the subsurface. Geological Survey of Denmark and Greenland Bulletin **38**, 13–16. *https://doi.org/10.34194/geusb.v38.4388*

Sha, L.P., Schwartz, C., van Lemberge, V.M., Cameron, T.D.J., Zöllmer, V., Konradi, P., Laban, C., Streif, H. & Schüttenhelm, Q. 1991: Quaternary Sedimentary Sequences in the southern North Sea basin. Sedimentology Working Group of Southern North Sea Project. In: Sha, L.P. (ed.): Final discipline report of the project: The Modelling and Dynamics of the Quaternary Geology of the Southern North Sea and their Applications to Environmental Protection and Industrial Developments. Commission of European Communities Rijks Geologische Dienst, Haarlem 135 pp: Directorate General, XII, Science Programme Contact No. SCI* 0128–C (EDB). *https://doi.org/10.13140/RG.2.1.4118.2803*

Steinicke, G. 1972: Endogene Tektonik in den Unter-Maastricht-Vorkommen auf Jasmund (Rügen). Geologie Supplement **71/72**, 207 pp.

Stewart, M.A., Lonergan, L. & Hampson, G. 2013: 3D seismic analysis of buried tunnel valleys in the central North Sea: morphology, cross-cutting generations and glacial history. Quaternary Science Reviews **72**, 1–17. *https://doi.org/10.1016/j.quascirev.2013.03.016*

van der Pluijm, B.A. & Marshak, S. 2004: Earth structure: An introduction to structural geology and tectonics. 2nd edition. 672 pp. WW Norton & Company, Inc., New York.

van der Wateren, D.F.M. 1985: A model of glacial tectonics applied to the ice-pushed ridges in the central Netherlands. Bulletin of the Geological Society Denmark **34**, 55–74. *https://doi.org/10.37570/bgsd-1985-34-06*

van der Wateren, D.F.M. 1995: Structural geology and sedimentology of push moraines. Medelingen Rijks Geologische Dienst **54**, 1–168.

Vaughan, D.P., Phillips, E., Lee, J.R. & Hart, J.K. 2024: A thin-skinned thrust model for ice-marginal glaciotectonic detachment and emplacement of Caboniferous bedrock rafts at Kilcummin Head, NW Ireland. Proceedings of the Geologists' Association **135**, 260–281. *https://doi.org/10.1016/j.pgeola.2024.04.001*

Vaughan-Hirsch, D.P. & Phillips, E.R. 2017: Mid-Pleistocene thin-skinned glaciotectonic thrusting of the Aberdeen Ground Formation, Central Graben region, central North Sea. Journal of Quaternary Science **32**(2), 196–212. *https://doi.org/10.1002/jqs.2836*

Wenau, S. & Alves, T.M. 2020: Salt-induced crestal faults control the formation of Quaternary tunnel valleys in the southern North Sea. Boreas **49**, 799–812. *https://doi.org/10.1111/bor.12461*

Wilkerson, M.S. & Dicken, C.L. 2001: Quick-look techniques for evaluating two-dimensional cross-sections in detached contractional settings. AAPG Bulletin **85**(10), 1759–1770.

Williams, D.G., Bramham, P.J., Eaton, G.P. & Harris, C. 2001: Late Devensian glaciotectonic deformation at St Bees, Cumbria: a critical wedge model. Journal of the Geological Society of London **158**, 125–135. *https://doi.org/10.1144/jgs.158.1.125*

Winsemann, J., Koopmann, H., Tanner, D.C., Lutz, R., Lang, J., Brandes, C. & Gaedicke, C. 2020: Seismic interpretation and structural restoration of the Heligoland glaciotectonic thrust fault complex: Implications for multiple deformation during (pre-) Elsterian to Warthian ice advances into the southern North Sea Basin. Quaternary Science Reviews **227**, 106068. *https://doi.org/10.1016/j.quascirev.2019.106068*

Yilmaz, Ö. 1987: Seismic data processing. In: Doherty S.M. (ed.): Investigation in Geophysics, Volume 2. Society of Exploration Geophysicists Investigations in Geophysics **2**, 526 pp. Tulsa, Oklahoma.